Chapter V

La and Sr Co-Doped Ceria, $Ce_{0.85}La_{0.15-x}Sr_xO_{2-\delta}$ and its Nanocomposites

This chapter consists of two sections. In the section1, effect of replacement of La^{3+} by Sr^{2+} in $Ce_{0.85}La_{0.15}O_{1.925}$ (molar concentration of oxygen vacancies changed) on the phases, structure and electrical properties has been discussed. The composition which shows the highest conductivity in this system has been chosen for the nanocomposites. Section 2 describes the effect of concentration of carbonates, $(Li_{0.52}Na_{0.48})_2CO_3$ on the phases, thermal, structural and electrical properties of La^{3+} and Sr^{2+} co-doped ceria.

5.1 La and Sr Co-Doped Ceria

5.1.1 Introduction

There is worldwide interest to reduce the operating temperature of SOFCs to 500-700 ^oC for long term stability [Stimming et al. (2002)]. This however, requires high ionic conductivity of the electrolytes in this temperature range. In order to increase the ionic conductivity, a co-doping approach has been used and found to be effective. Herle et al. (1999) found that co-doping of ceria with aliovalent cations such as rare earth and alkaline earth ions showed significantly higher ionic conductivity than the singly doped ceria electrolytes. Some co-doped ceria electrolytes reported in the literature are $Ce_{1-x-y}Sm_xCa_yO_{2-\delta}$ [Mori et al. (2002)], $Ce_{0.80}Sm_{0.20-x}Y_xO_{2-\delta}$ [Sha et al. (2006)], $Ce_{1-x}Sm_{0.15-x}Gd_xO_{1.925}$ [Singh et al. (2012)], $Ce_{0.85}Gd_{0.10}Mg_{0.05}O_{2-\delta}$ [Wang et al. (2004)], and $Ce_{1-x-y}Gd_xPr_yO_{2-\delta}$ [Lubke et al. (1999)]. Zheng et al. (2009) studied the electrical properties of $Ce_{0.80}Sm_{0.20-x}Mg_xO_{2-\delta}$ samples synthesized by solid state reaction by sintering at 1550 ^oC. They found that substitution of Mg for Sm up to 50 mol% slightly increases the conductivity as compared to that of ceria doped with Sm only. Zheng et al. (2009A) studied the electrical properties of $Ce_{1-x}La_{x-y}Ca_yO_{2-\delta}$ and observed that the composition $Ce_{0.85}La_{0.10}Ca_{0.05}O_{2-\delta}$ has the maximum conductivity (3.56×10^{-2} at 700 ^oC) of all the compositions. Cioatera et al. (2009) studied the effect

of addition of Sr on the properties of europium doped ceria. It was found that an optimum ratio of europium/strontium increased the conductivity due to decrease in the grain boundary resistance. Some other co-doped ceria electrolytes studied are $Ce_{0.80-x}Sm_{0.20}Sr_xO_{2-\delta}$ [Tsung et al. (2007)], $Ce_{0.80-x}Gd_{0.20}Sr_xO_{2-\delta}$ [Ramesh et al. (2009)] and $Ce_{0.80}Y_{0.20-x}Sr_xO_{2-\delta}$ [Zheng et al. (2009B)]. An improvement in the conductivity has been found in these systems due to decrease in the resistance of the grain boundaries. In chapter 4, effect of strontium addition on the conductivity of singly La doped ceria ($Ce_{0.85}La_{0.15}O_{1.925}$) keeping total number of oxygen vacancies constant has been reported. In this chapter, La and Sr co-doped ceria viz $Ce_{0.85}La_{0.15-x}Sr_xO_{\{2-(0.075+x/2)}$ [(x=0.0; CLO15), (x=0.025; CL125S025), (x=0.05; CL10S5) and (x=0.075, CL075S075)] have been prepared and characterized to study the effect of increasing oxygen vacancies on the ionic conductivity by changing the concentration of Sr. It is considered worthwhile to study the ionic conductivity of these materials because if these have more or comparable conductivity with Sm or Gd-doped ceria as mentioned above, their use will reduce the cost of SOFCs.

5.1.2 Results and discussion

(a) Crystal structure and phases

Powder XRD patterns of all the calcined and sintered samples are recorded to check the phase purity of powder and to determine the crystal structure. XRD patterns of the calcined powders show broad peaks. Diffraction patterns are indexed on the basis of fluorite structure similar to CeO_2 using JCPDS file no. 43-1002. Average crystallite size of the calcined powders determined by Scherrer's formula is given in Table.5.1. Fig. 5.1 shows powder XRD patterns of the sintered samples. It has been observed that peaks corresponding to (111) and (200) planes shift slightly toward lower 2θ angle with increasing Sr content (x). This indicates that unit cell of co-doped ceria expands with increasing concentration of Sr. Lattice parameters of various compositions determined by non-linear least square fitting of the X-ray data using 'Unit Cell' program are given in Table. 5.1.

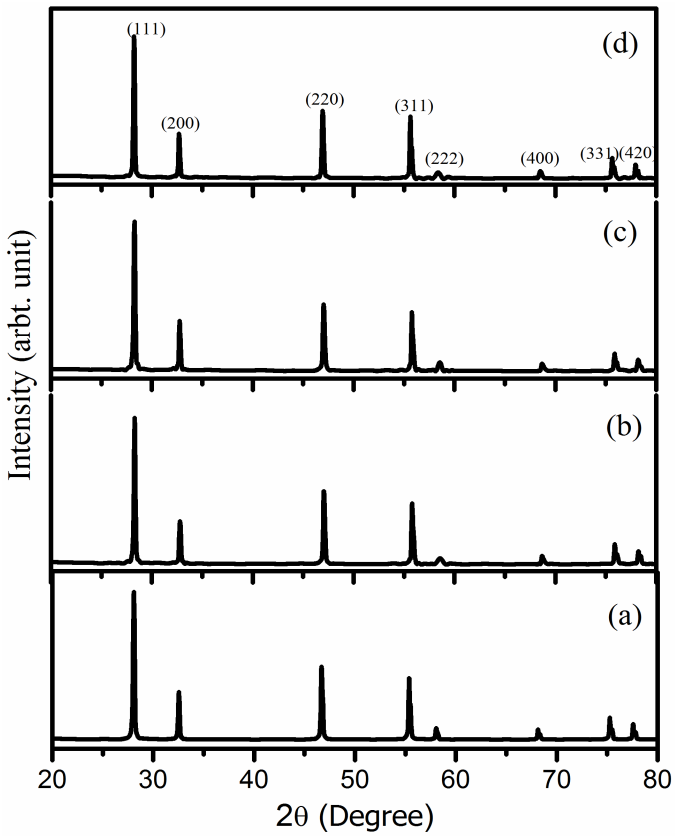

Fig. 5.1 Powder X-ray diffraction patterns of the sintered powders in the system $Ce_{0.85}La_{0.15-x}Sr_xO_{\{2-(0.075+x/2)\}}$ for (a) CLO15 (b) CL125S025 (c) CL10S5 and (d) CL075S075

Increase in the lattice parameter on substitution of La^{3+} and Sr^{2+} is attributed to larger ionic radius of La^{3+} (1.16 Å) and Sr^{2+} (1.26 Å) as compared to Ce^{4+} (0.97 Å) [Shannon R. (1976)]. It can be seen that lattice parameter increases linearly with increase in Sr content following Vegard's law [Vegard et al. (1928)]. This variation can be represented as:

$$a(x) = 0.54578 + 0.0892x \quad (5.1)$$

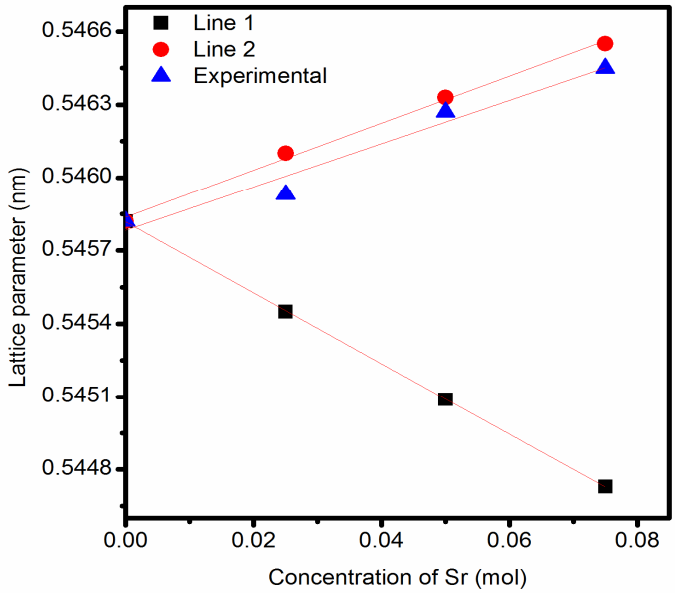

Fig. 5.2 Variation of lattice parameter with concentration of Sr in the system $Ce_{0.85}La_{0.15-x}Sr_xO_{\{2-(0.075+x/2)\}}$

Variation of lattice parameter with strontium concentration is shown in Fig. 5.2. Theoretical values of lattice parameter determined using hard sphere model (Eq. 4.6 in Chapter 4) are also plotted in Fig. 5.2.

Table. 5.1 Crystallite size (calcined powders), lattice parameter and % theoretical density of compositions of the system $Ce_{0.85}La_{0.15-x}Sr_xO_{\{2-(0.075+x/2)\}}$

S. No.	x	Sample code	Crystallite size (nm)	Lattice parameter (Å)	% T D
1.	0.0	CLO15	21	5.4582+/-0.0005	98.3
2.	0.025	CL125S025	24	5.4650+/-0.0004	98.2
3.	0.05	CL10S5	26	5.4760+/-0.0007	97.0
4.	0.075	CL075S075	25	5.4891+/-0.0009	95.0

Line1 shows the results when the values of $r_{V_{O_i}^{\cdot\cdot}}$ and $r_{V_{O_d}^{\cdot\cdot}}$ have been substituted as 1.154 and 0.9498 Å respectively in Eq. 4.6 (Chapter 4). Line 2 shows the values when the average radius of oxygen vacancies (1.16 Å) was used in Eq. 4.6 (Chapter 4). It can be observed from Fig. 5.2 that the experimental values and the values shown by line 2 follow the same trend i.e. lattice parameter increases with increasing the concentration of Sr^{2+}. It is also noticed that these values are close to each other. Sintered pellets have density more than 95% of the theoretical values (Table 5.1).

(b) Microstructure

Typical bright field transmission electron micrographs (BF-TEM) of the calcined powder of all the compositions in the system, $Ce_{0.85}La_{0.15-x}Sr_xO_{\{2-(0.075+x/2)\}}$ are shown in Fig. 5.3 (i)-(iv). These images clearly indicate that some particles are spherical and some are faceted and agglomerated particles are also present. TEM images show that average crystallite size lies in the range 18-30±4 nm. This is in good agreement with the results obtained from Scherrer's formula (given in Table.5.1).

Figs. 5.4 (a)-(d) show scanning electron micrographs of the sintered samples. Micrographs reveal a dense structure and well defined grains separated by the grain boundaries. All the samples have grains of varying size. It is observed that the average grain size increases with increasing concentration of Sr. Average grain size is found to be 1.0, 2.0, 4.5, and 5 μm for the samples with x = 0.0, 0.025, 0.05 and 0.075 respectively.

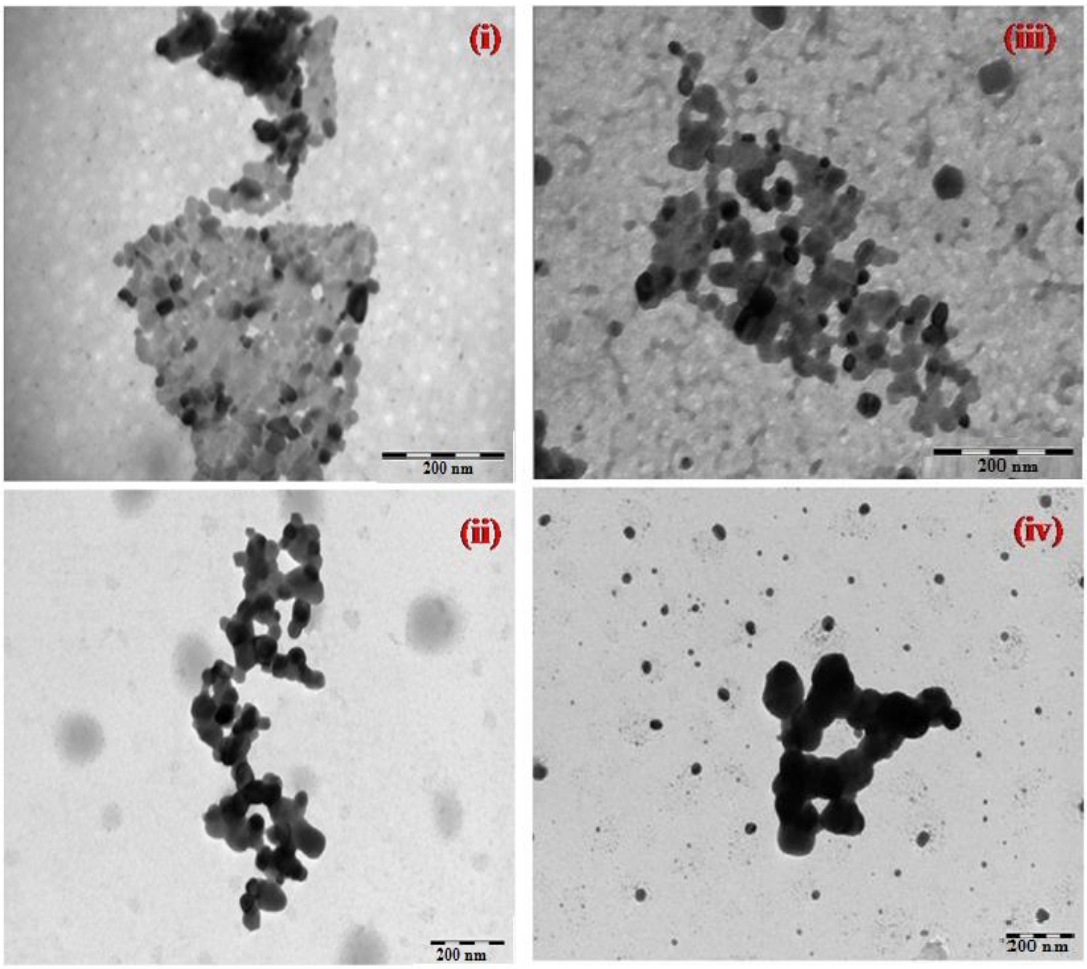

Fig. 5.3 BFTEM images of the compositions (i) CLO15 (ii) CL125S025 (iii) CL10S5 (iv) CL075S075

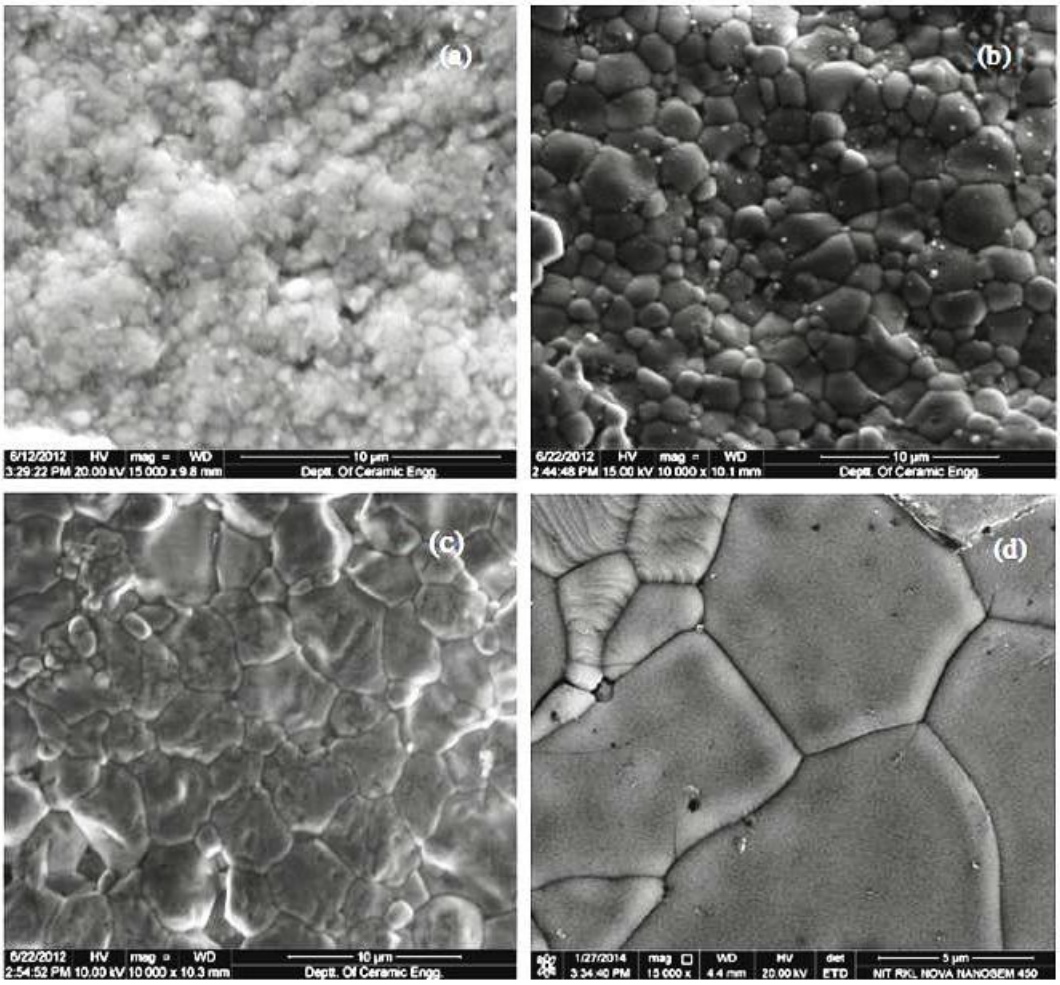

Fig. 5.4 SEM micrographs of different compositions in the system $Ce_{0.85}La_{0.15-x}Sr_xO_{\{2-(0.075+x/2)\}}$ (a) CLO15 (b) CL125S025 (c) CL10S5 and (d) CL075S075

Fig. 5.5 shows the EDS spectrum of the composition, CL125S025 at three points in the micrograph. It can be observed from the spectrum that all the constituent elements are present. Spectrum of the grain, the grain boundary and the triple point is the same except that a second phase of some silicate is present at the triple point. Si is present at the grain boundary in the case of CLO15 [Fig. 4.5, Chapter 4]. In the case of composition CL125S025, Sr reacts with silica and forms some silicate phase which segregates at the triple point.

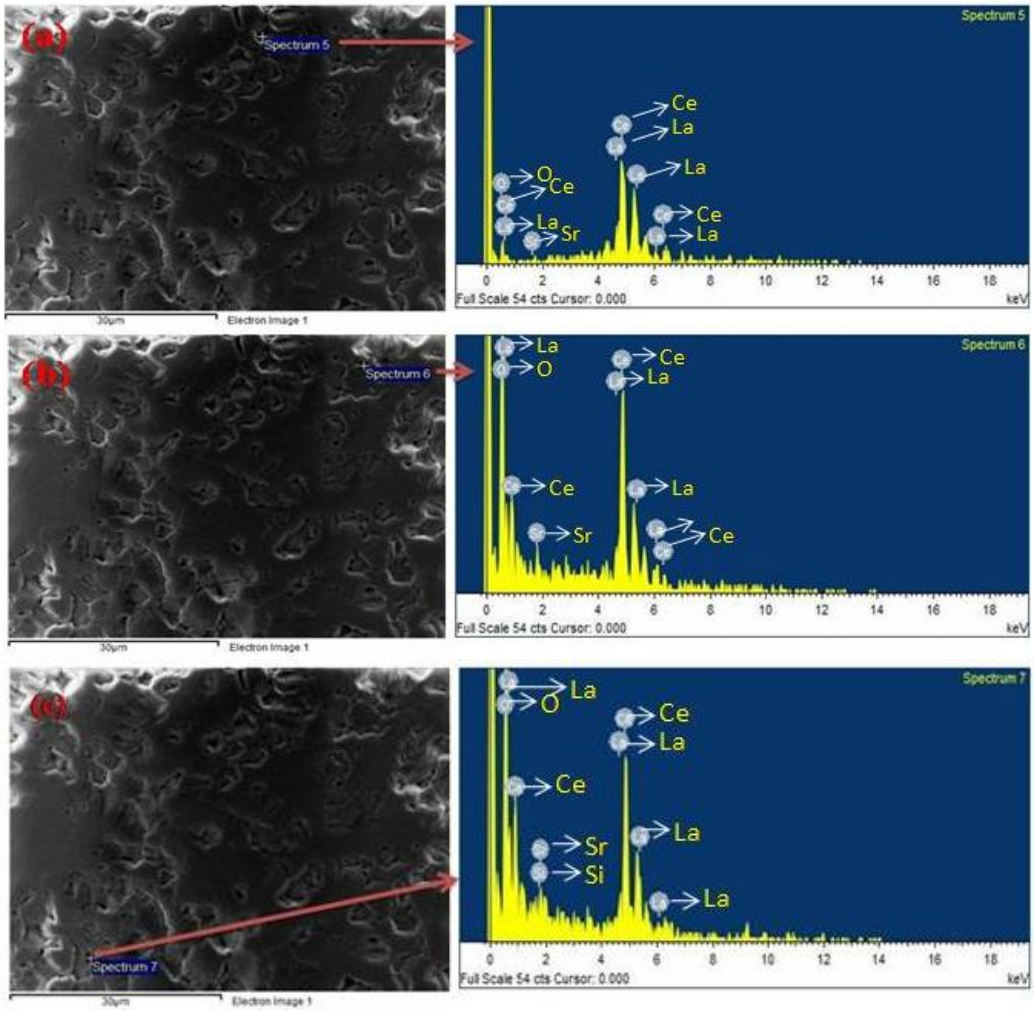

Fig. 5.5 EDS spectrum of the composition CL125S025 at three different points in the sample: (a) in the grain (b) at the grain boundary and (c) at the triple point

This leaves clean grain boundaries for grain to grain contact leading to easy diffusion of O^{2-} ions across the grain boundaries. The composition, morphology and distribution of these phases needs to be determined using STEM combined with EDXM and EELS [Grehardt et al. (1986)].

(c) Electrical conductivity

Complex plane impedance plots of compositions CL125S025, CL10S5 and CL075S075 at different temperatures are shown in Figs. 5.6-5.8. In case of CLO15 two depressed circular arcs have been observed at 200 °C (Fig.4.7, Chapter 4). For the composition, CL125S025, three depressed circular arcs have been observed at 200 ºC. The arc passing through the origin in the higher frequency range is ascribed to the contribution of the grains. The arc in the intermediate frequency range is ascribed to the contribution of the grain boundaries. A spike in the low frequency region is observed due to electrode/specimen interface polarization. The grains and grain boundaries arcs are associated with the capacitance in the pF (10^{-10}-10^{-12}) and nF (10^{-7}-10^{-9}) ranges [Hodge et al. (1976)] respectively. These are determined from the relation: $2\pi f_{max}RC = 1$, where f_{max} is the frequency at the highest point of the arc and R is the resistance and C is the capacitance of a particular contribution. The relaxation frequency of any particular polarization process increases with increasing temperature. Therefore, the arcs corresponding to the grains and grain boundaries disappear above 300 and 425 ºC respectively. Only the arc due to electrode has been observed at higher temperatures. It can also be noted from Fig. 5.6 that arc of the grain boundaries is smaller than that of CLO15 (Fig. 4.7).

Impedance plots are fitted to an equivalent circuit to determine the resistance of the grains and the grain boundaries. In the present investigation, only arcs of the grains and the grain boundaries are fitted to determine their respective contribution. The contribution of the electrode arc is not considered because the sum of resistance of the grains and the grain boundaries is equal to the total resistance of the sample.

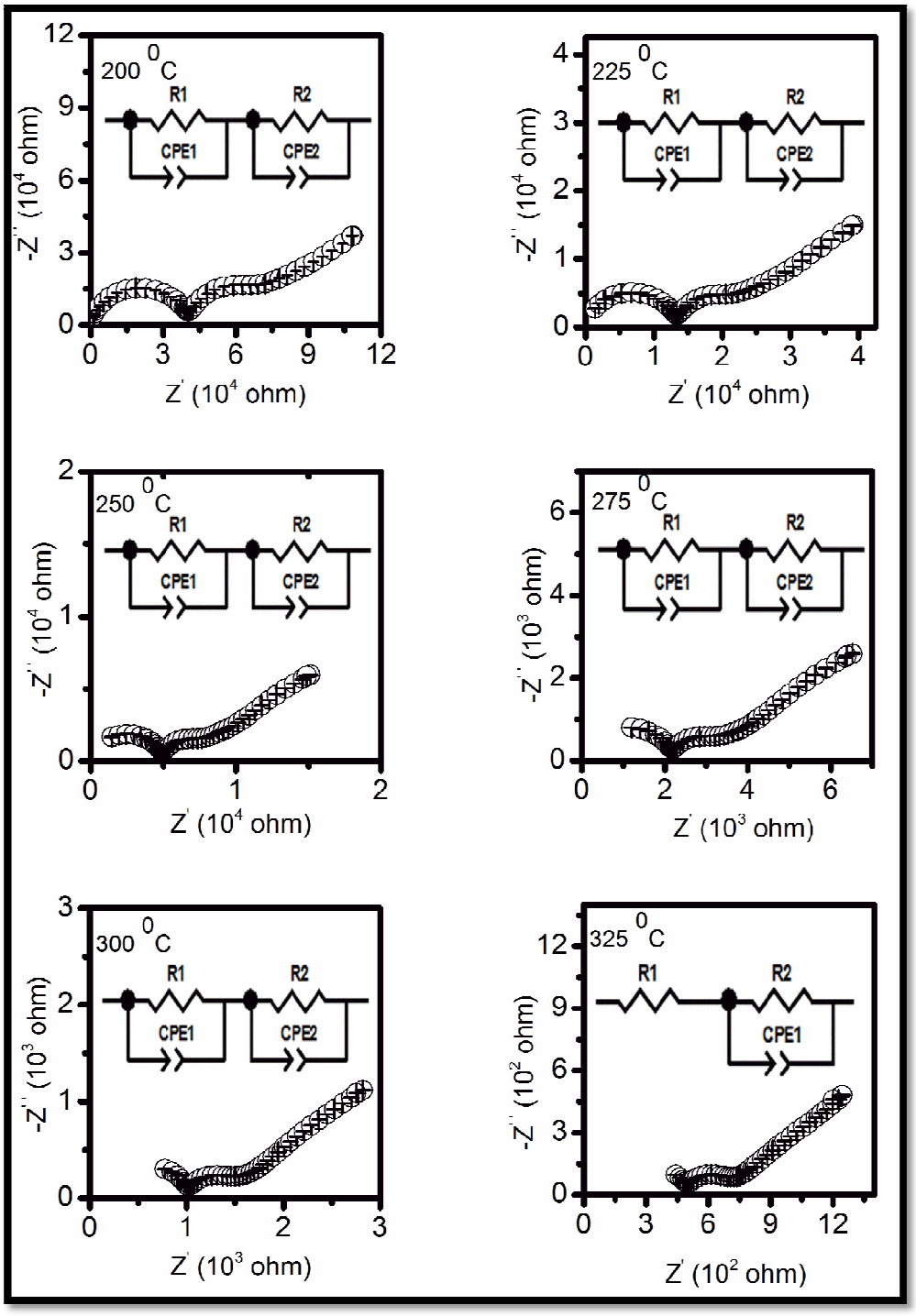

Fig. 5.6 Complex plane impedance plots of the composition CL125S025 at different temperatures

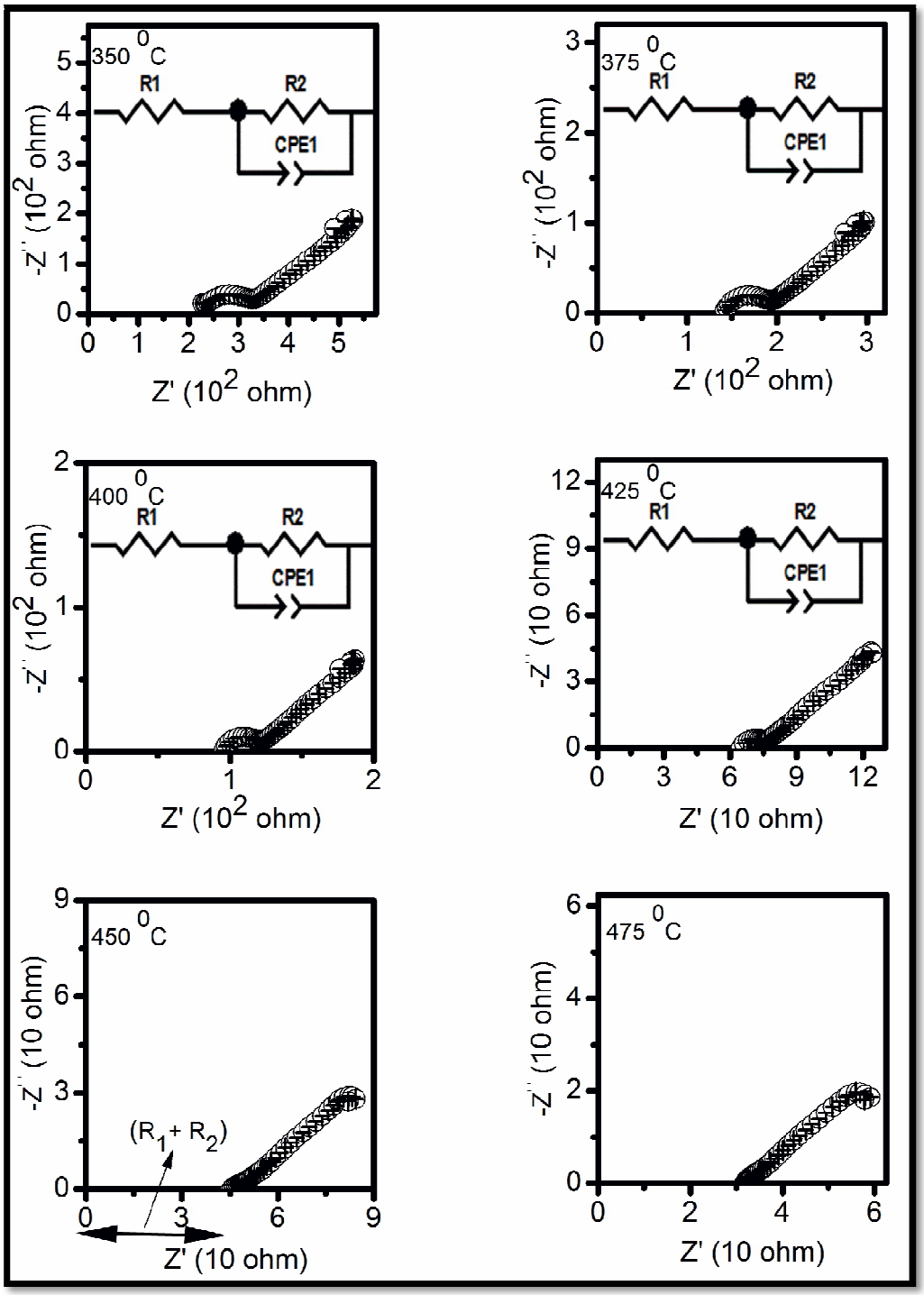

Fig. 5.6 Complex plane impedance plots of the composition CL125S025 at different temperatures

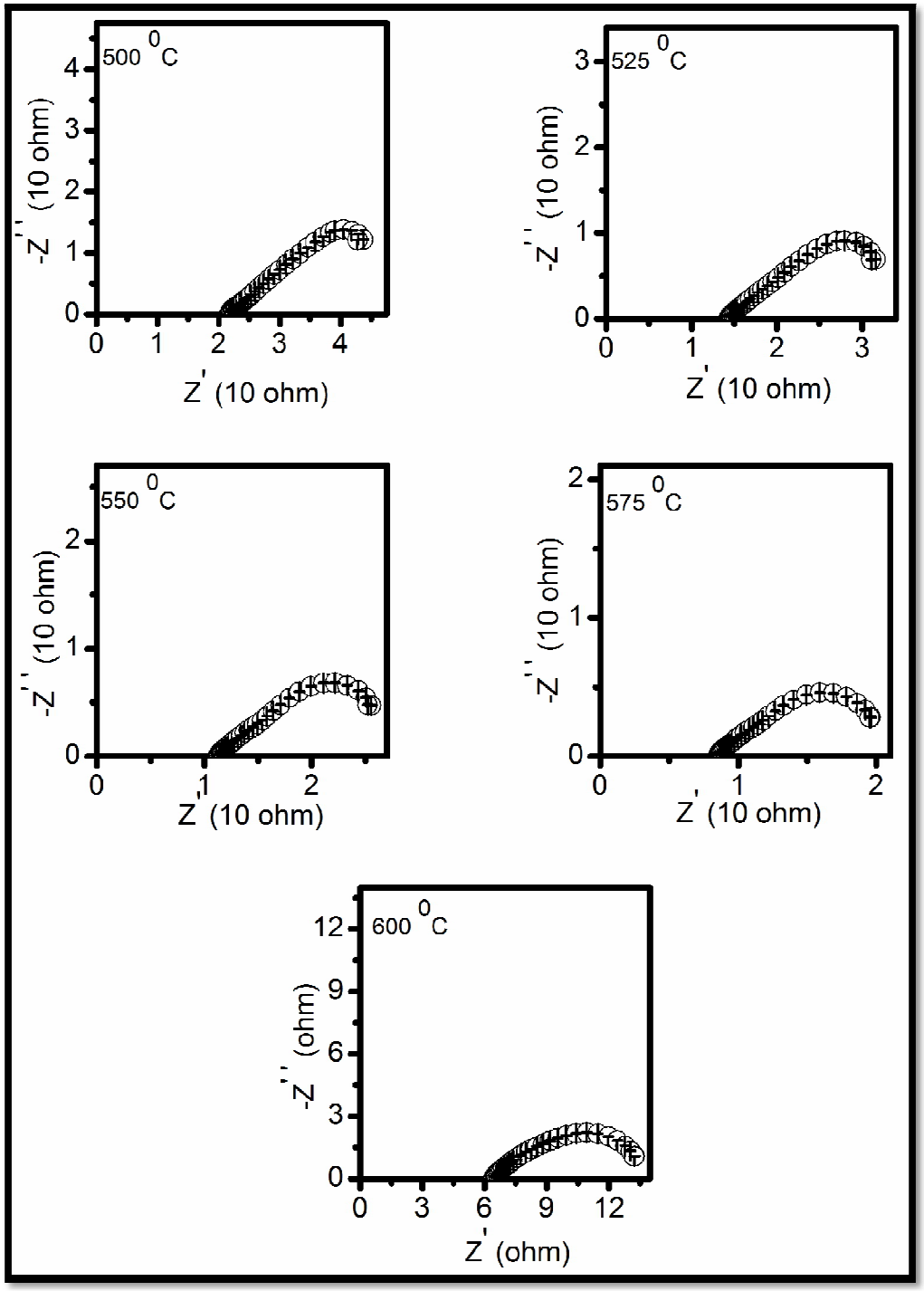

Fig. 5.6 Complex plane impedance plots of the composition CL125S025 at different temperatures

For composition, CL10S5, three depressed arcs are seen in the temperature range 200-350 ºC (Fig. 5.7). The arcs ascribed to the contribution of the grains and the grain boundaries disappear above 350 and 425 ºC respectively. To see clearly the contribution of the grain boundaries above 325 ºC, the data is plotted in the insets. At higher temperatures, only low frequency arc has been observed. Beyond 425 ºC, the total resistance of the electrolyte has been determined by the intercept on the higher frequency side of the electrode arc on the real ($Z^{'}$) axis.

In the case of composition, CL075S075, three depressed arcs are present in the temperature range 200-350 ºC (Fig. 5.8). High and intermediate frequency arcs disappear above 325 and 450 ºC respectively due to increase in the relaxation frequency with the temperature. Data are plotted in the insets to see clearly the value of resistance of the grain boundaries at higher temperatures.

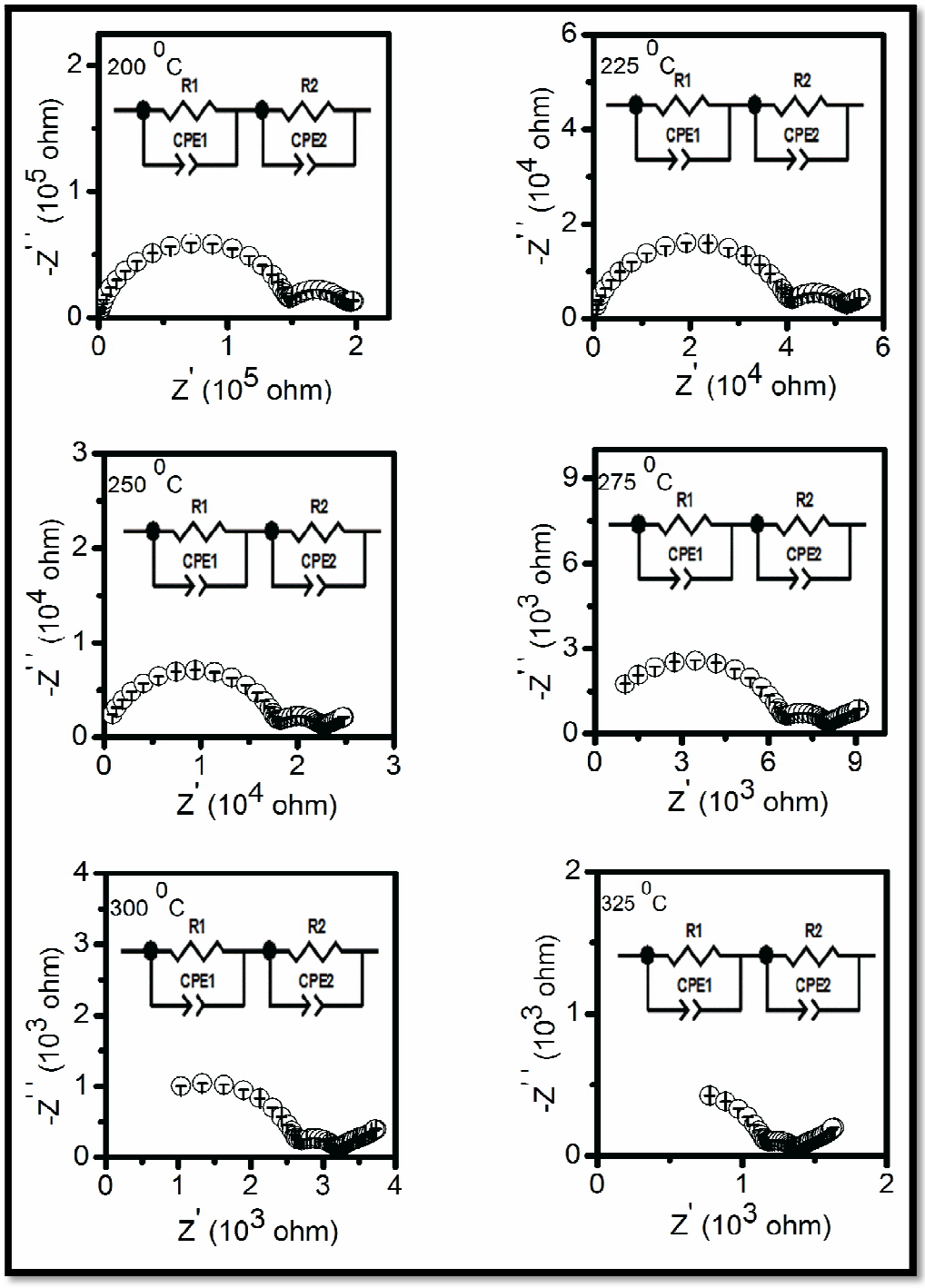

Fig. 5.7 Complex plane impedance plots of the composition CL10S5 at different temperatures

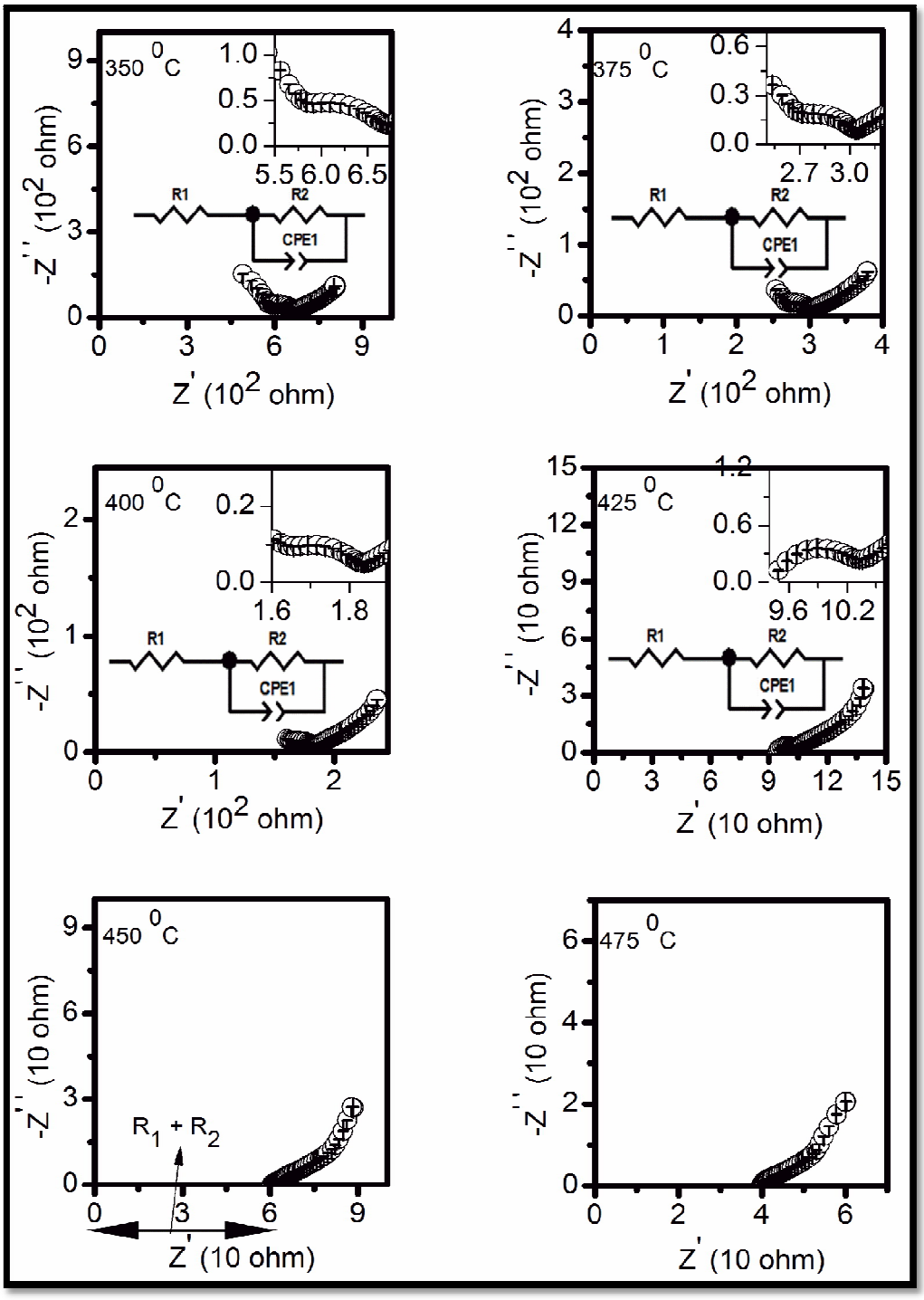

Fig. 5.7 Complex plane impedance plots of the composition CL10S5 at different temperatures

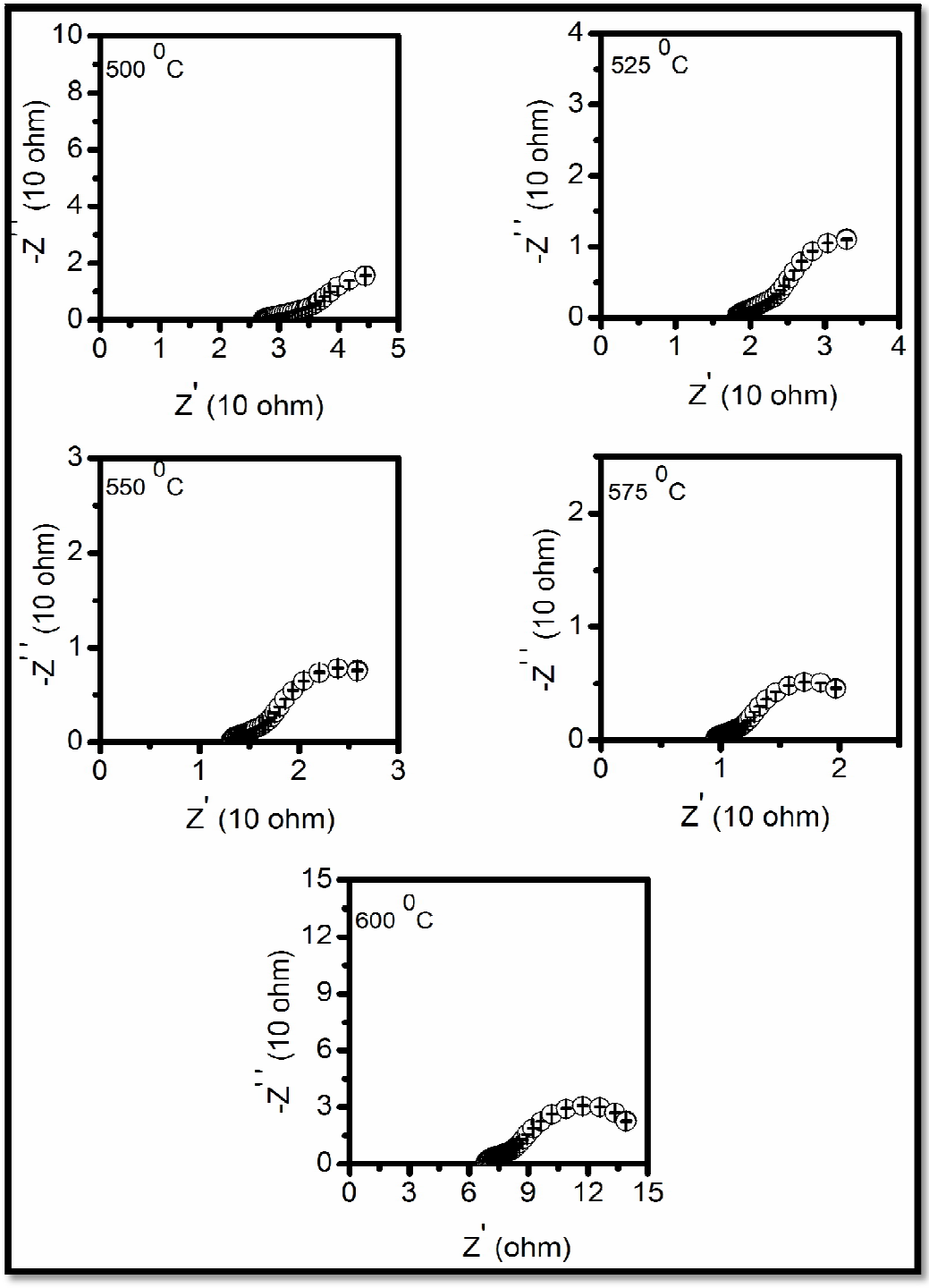

Fig. 5.7 Complex plane impedance plots of the composition CL10S5 at different temperatures

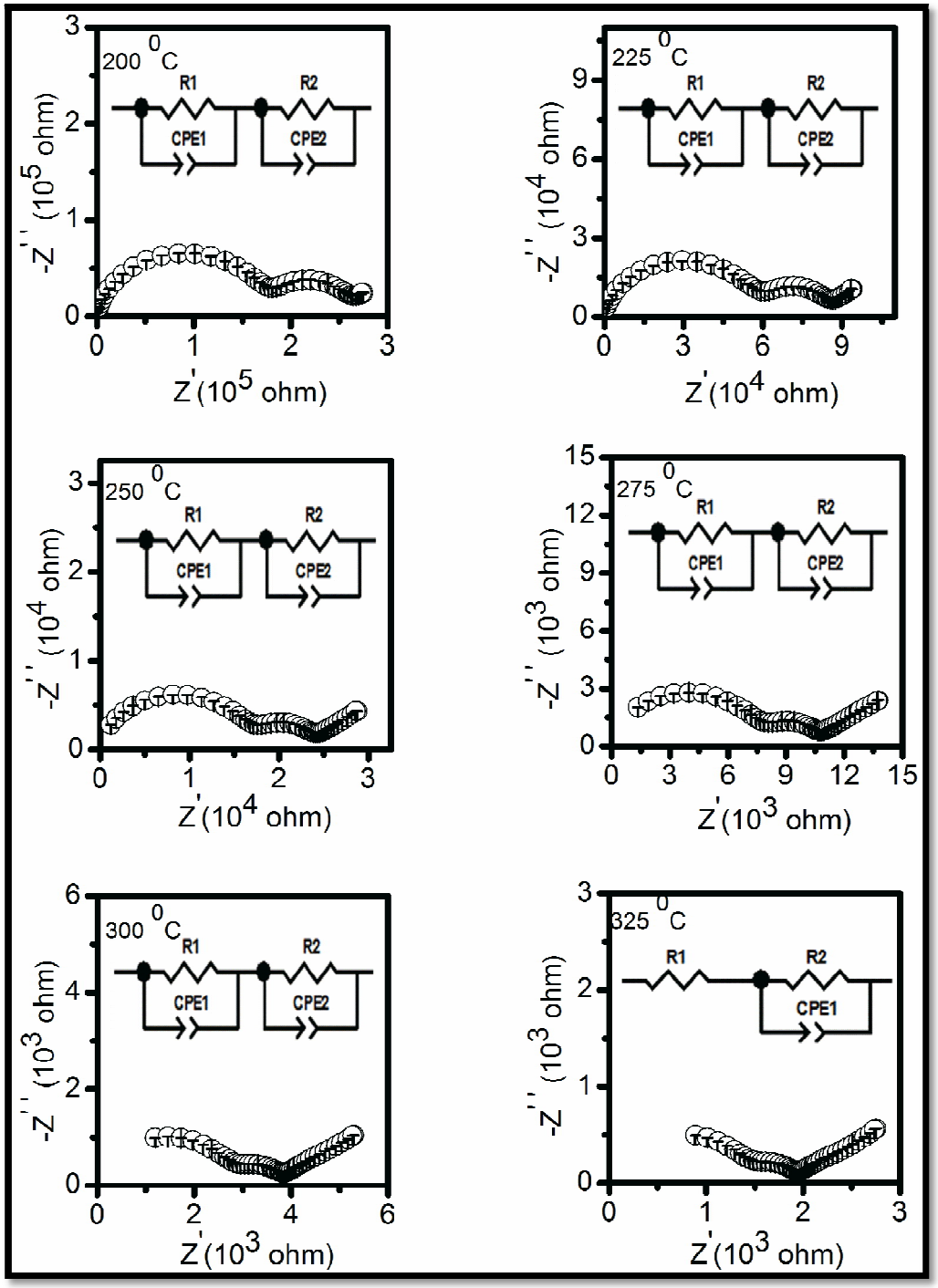

Fig. 5.8 Complex plane impedance plots of the composition CL075S075 at different temperatures

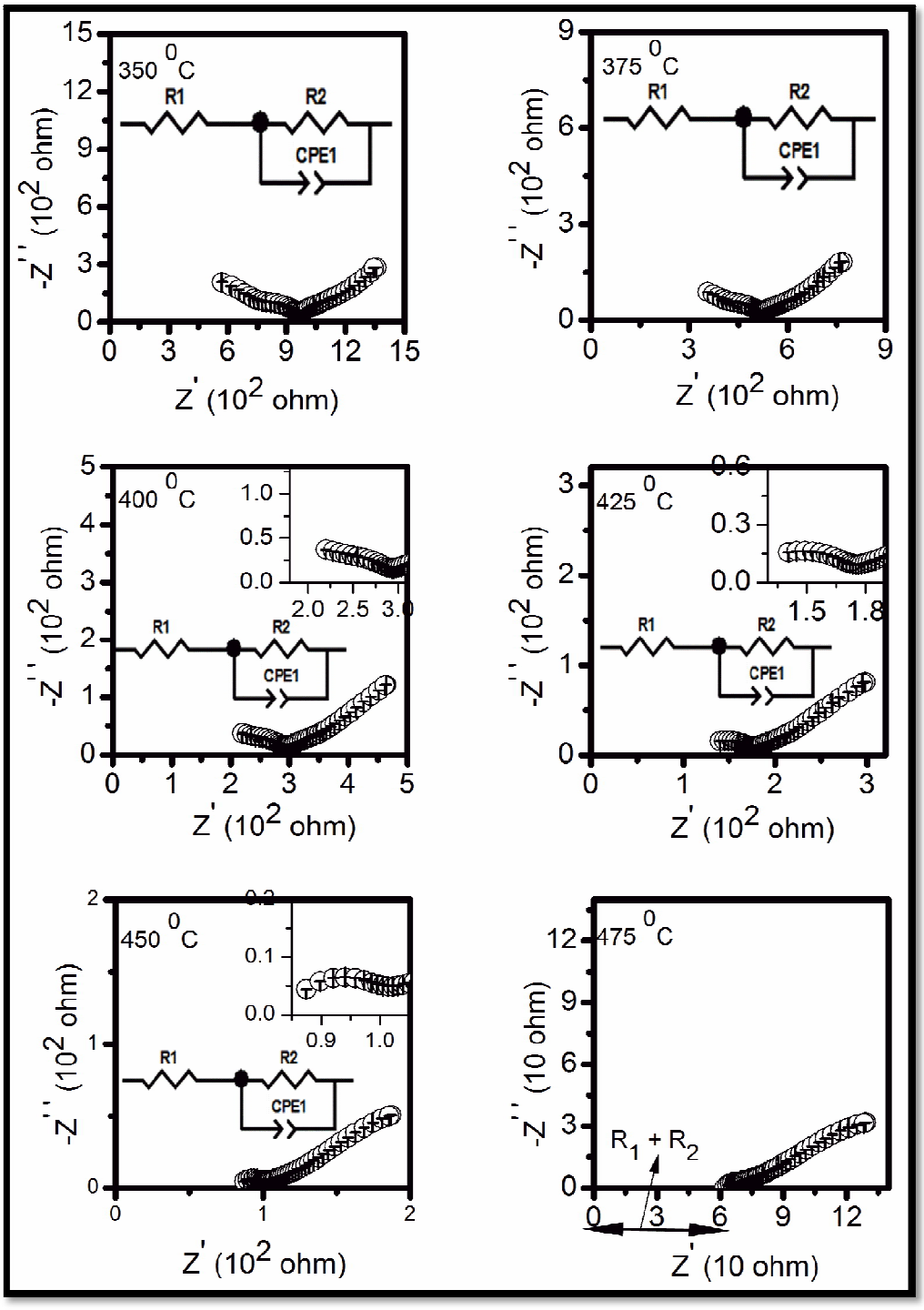

Fig. 5.8 Complex plane impedance plots of the composition CL075S075 at different temperatures

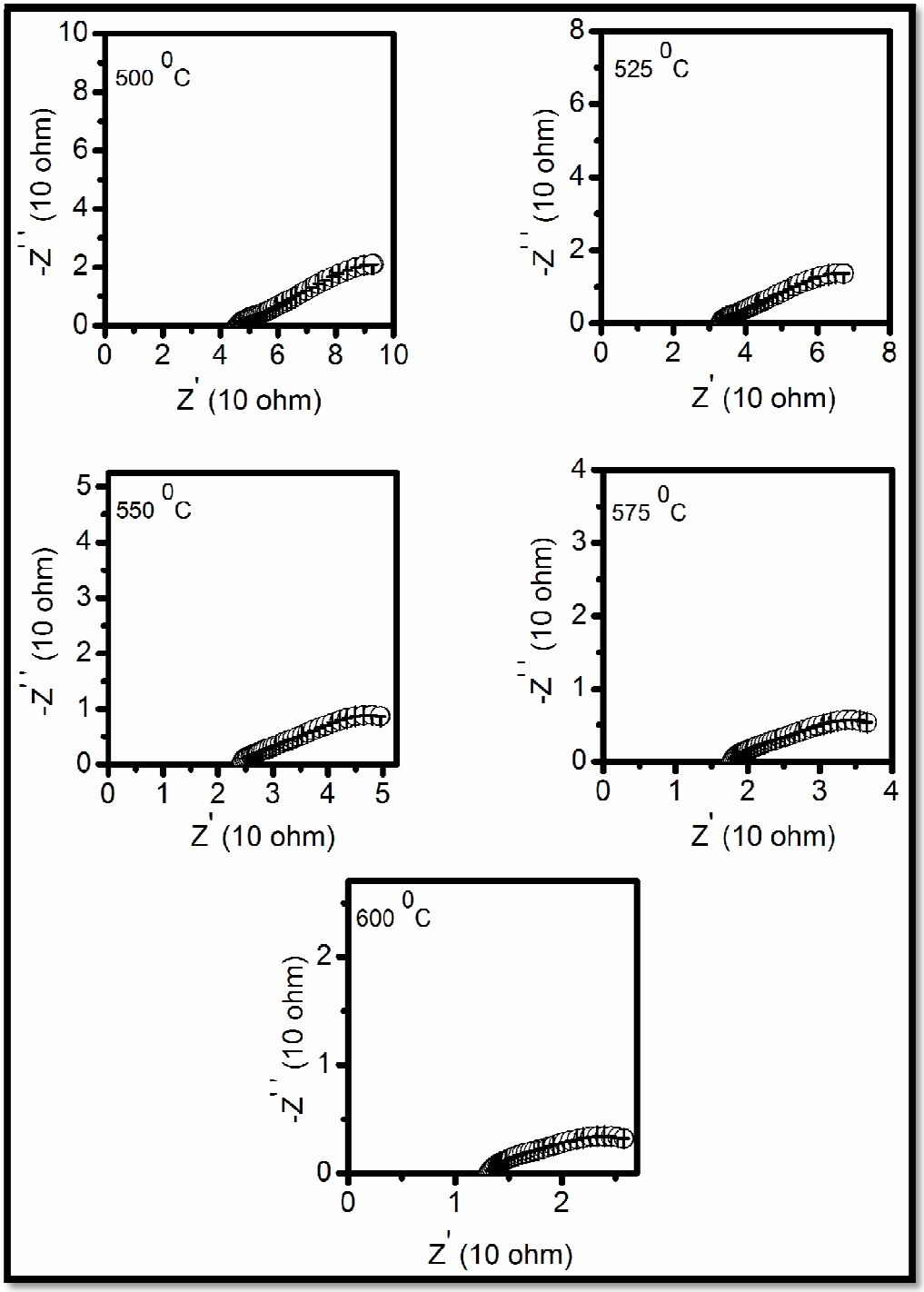

Fig. 5.8 Complex plane impedance plots of the composition CL075S075 at different temperatures

Arrhenius plots for the grains (bulk), grain boundaries and total conductivity are shown in Fig. 5.9. It can be seen from Fig. 5.9 that the bulk conductivity increases for the composition CL125S025 followed by a decrease at higher concentration of Sr^{2+}. The enhancement in the bulk conductivity is ascribed to an increase in the number of oxygen vacancies and suppression of ordering of oxygen vacancies i.e. increase of configurational entropy. This leads to a decrease in the activation energy for diffusion of O^{2-} ions and increases the conductivity. Table. 5.2 shows the values of configurational entropy (S) of all the samples. Co-doped samples have higher value of S than that of CLO15 and it is also higher than the values of S obtained in the Chapter 4 i.e. when the concentration of oxygen vacancies is kept constant. Values of S increase with increasing the concentration of Sr. The bulk conductivity starts decreasing at higher concentration (x > 0.025) of Sr^{2+}. It may be due to increase in the number of neutral associated defect pairs $[Sr''_{Ce}\text{-}V_O^{\bullet\bullet}]^x$ which reduces the number of free oxygen vacancies and hence decrease the conductivity [Ciotera et al. (2009)]. It can be concluded that criteria of configurational entropy applies up to x = 0.025. Beyond this concentration, other factors (given below) start dominating. This decreases the conductivity.

Arrhenius plots for the bulk conductivity of co-doped samples show a change in the slope at 350 ^oC. It is interpreted as a transition from associated defect pairs (region where the oxygen vacancies are bound to the dopant site) to dissociated defects (region where oxygen vacancies are free). In the low temperature range activation energy (E_a) is equal to the sum of migration enthalpy (E_M) and association enthalpy (E_A) and in the high temperature region it is equal to migration enthalpy only. At low temperatures concentration of charge carriers is determined by the thermodynamic equilibrium between the free defects and associated defect pairs viz. $[La'_{Ce}\text{-}V_O^{\bullet\bullet}]^{\bullet}$ and $[Sr''_{Ce}\text{-}V_O^{\bullet\bullet}]^x$. Activation energy of conduction for the grains, E_g, has been determined using Arrhenius relationship:

$$\sigma_g T = \frac{\sigma_{0g}}{T} \, exp\left(-\frac{E_g}{kT}\right) \qquad (5.1)$$

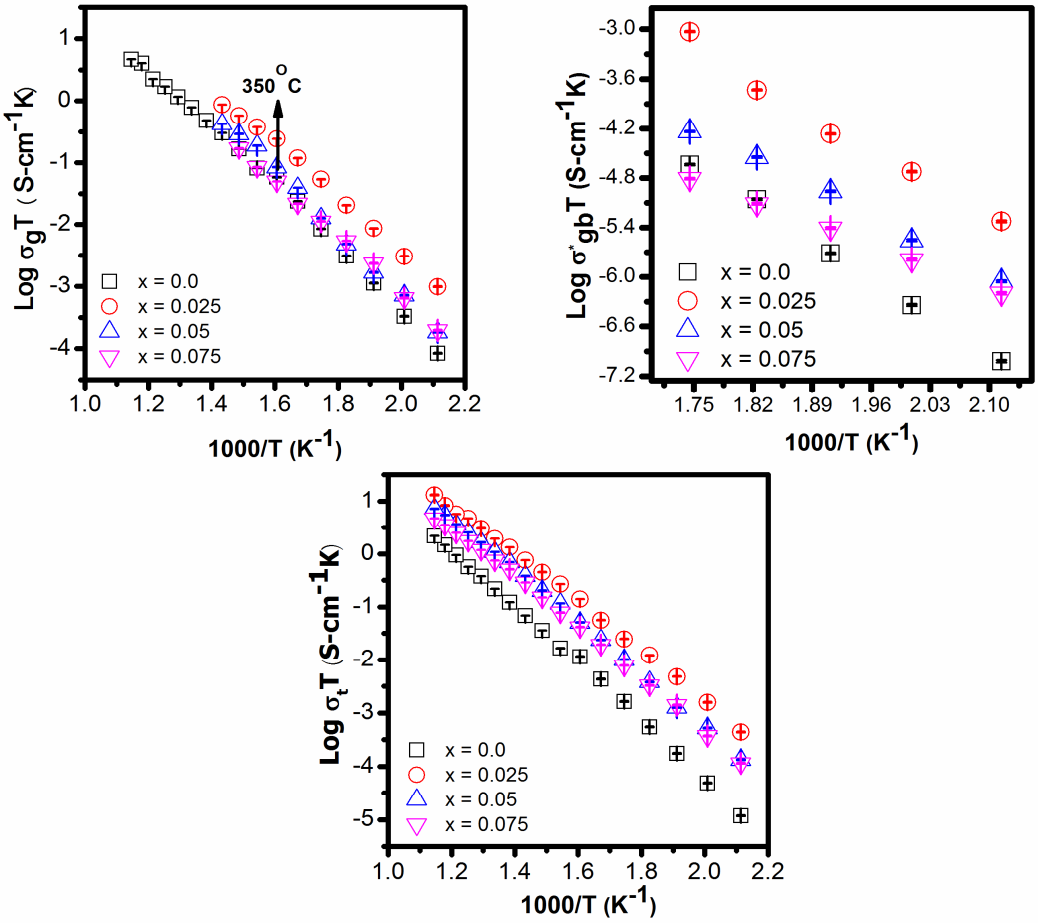

Fig. 5.9 Arrhenius plots for the grains, grain boundaries and total ionic conductivity in the system $Ce_{0.85}La_{0.15-x}Sr_xO_{\{2-(0.075+x/2)\}}$

where, σ_{0g} is the pre exponential factor, k is the Boltzmann constant and T is absolute temperature. Values of E_g, for all the samples determined by fitting the data in Fig. 5.9 to equation (5.1) are given in Table 5.3. Activation energy for the bulk conductivity of co-doped samples is less than that of CLO15. It is also noted from Table. 5.3 that activation energy is more at low temperature and less at higher temperatures.

Arrhenius plots for the conductivity of the grain boundaries show that co-doped samples have higher grain boundaries conductivity than that of singly La doped ceria.

This clearly shows that doping with Sr has a significant influence on the conductivity of grain boundaries. This may be due to scavenging effect of strontium which removes siliceous impurities present at the grain boundaries. Sr^{2+} reacts with silica present at the grain boundaries to form a second phase. This phase segregates at triple point junction rather than being present entirely on the grain boundaries. Therefore, majority of the grain boundaries become free from the resistive silicate phases. This increases the conductivity of grain boundaries substantially. Values of blocking factor, α_{gb} for all the samples are given in Table. 5.2. For the composition CL125S025, α_{gb} has been found to be 0.29 which is much less than the value 0.90 obtained for CLO15. Therefore, it is concluded that strontium is an effective grain boundary scavenger.

It is also observed that grain boundaries conductivity increases with decreasing average grain size of the co-doped samples. This is because for small grain size there is larger area of the grain boundaries. The finite amount of impurity contained in the sample is not sufficient to form a continuous and uniform glassy phase layer along the grain boundaries. This leaves the remaining grain boundaries area for clean grain to grain contact [Tian et al. (2000)]. Therefore, the transport of O^{2-} ions becomes faster across the grains through clean grain boundaries.

Activation energy of conduction for the grain boundaries, E_{gb} was determined by fitting the data in Fig. 5.9 to Arrhenius equation (Table. 5.3).

$$\sigma_{gb}T = \frac{\sigma_{0gb}}{T} \exp\left(-\frac{E_{gb}}{kT}\right) \quad (5.2)$$

Plots of Log $\sigma_t T$ vs 1000/T show that the co-doped samples have higher total ionic conductivity than that of CLO15. Composition containing 2.5 mol% of Sr has the highest ionic conductivity and lowest activation energy (E_t) of all the compositions. On further increasing the concentration of Sr, the total conductivity (σ_t) decreases. Values of the activation energy of total ionic conductivity, E_t, determined by fitting the data points in Fig. 5.9 to Eq. 5.3 are given in Table. 5.3.

$$\sigma_t T = \frac{\sigma_{0t}}{T} exp\left(-\frac{E_t}{kT}\right) \quad (5.3)$$

Values of σ_t of all the compositions at 600 ^oC are given in Table. 5.2. Conductivity of composition, CL125S025 is 1.50×10^{-2} S/cm at 600 ^oC.

Table. 5.2 Total conductivity (σ_t) at 600 ^oC, configurational entropy (S) and blocking factor (α_{gb}) of various compositions in the system $Ce_{0.85}La_{0.15-x}Sr_xO_{\{2-(0.075+x/2)\}}$

S. No.	x	Sample code	σ_t (S/cm) at 600 ^oC	S (J/mol-K)	α_{gb}
1.	0.0	CLO15	2.50×10^{-3}	3.50	0.90
2.	0.025	CL125S025	1.50×10^{-2}	4.06	0.29
3.	0.05	CL10S5	8.19×10^{-3}	4.30	0.38
4.	0.075	CL075S075	5.37×10^{-3}	4.37	0.25

This value is higher than the highest values reported for the compositions $Ce_{0.8}La_{0.14}Y_{0.06}O_{1.9}$ (6.1×10^{-3} S/cm) [Sha et al. (2007)] $Ce_{0.80}Sm_{0.20}O_{1.90}$ (SDC) (1.20×10^{-2} S/cm) [Balazas et al. (1995)] and $Ce_{0.80}Gd_{0.20}O_{1.90}$ (GDC) (1.29×10^{-2} S/cm) [Fu et al. (2010)] at 600 ^oC. This may make it a potential candidate as a solid electrolyte for IT-SOFCs. Its cost is definitely much less than the cost of CeO_2 singly doped with Sm and Gd as mentioned above. This is because La_2O_3 is cheaper than Sm_2O_3 and Gd_2O_3.

Partial replacement of La with Sr in CeO_2 has some opposite effects. It leads to increase in the number of oxygen vacancies. Ordering of oxygen vacancies is suppressed due to co-doping causes an increase in the configurational entropy [Yamamura et al. (2000)]. This leads to decrease in the activation energy for conduction and increases the ionic conductivity. Sr^{2+} also acts as a grain boundaries scavenger.

Table. 5.3 Activation energy of conduction for the grains (E_g), the grain boundaries (E_{gb}) and total (E_t) conductivity and blocking factor (α_{gb}) of various compositions in the system $Ce_{0.85}La_{0.15-x}Sr_xO_{\{2-(0.075+x/2)\}}$

S. No.	x	Sample code	E_g (eV) (200-350 °C)	E_g (eV) (350-600 °C)	E_{gb} (eV)	E_t (eV)
1.	0.0	CLO15	1.01 (200-600 °C)		1.30	1.06
2.	0.025	CL125S025	0.94	0.65	1.07	0.91
3.	0.05	CL10S5	1.03	0.70	0.99	0.98
4.	0.075	CL075S075	1.04	0.64	0.80	0.95

This decreases the grain boundaries resistance and hence increases the grain boundaries conductivity as well as the total conductivity. Number of associated defects pairs and their association energy increase with increasing Sr^{2+} substitution. This leads to decrease in the ionic conductivity. Deviation of lattice parameter on substituting La^{3+} and Sr^{2+} from that of undoped ceria increases the strain in the lattice because ionic radius increases in the order $Ce^{4+} < La^{3+} < Sr^{2+}$ [Kim (1989)]. This increases the activation energy for diffusion of O^{2-} ions. Due to complex interplay of these opposite competiting effects, conductivity increases up to x = 0.025 followed by a decrease at higher concentration i.e. x > 0.025.

5.1.3 Conclusion

- Co-doped ceria samples with nominal compositions $Ce_{0.85}La_{0.15-x}Sr_xO_{\{2-(0.075+x/2)\}}$ where, x = 0.0, 0.025, 0.050 and 0.075 have been synthesized successfully using citrate nitrate gel auto-combustion route.
- Single phase solid solution has formed in all the compositions.

- More than 95% of the theoretical density has been achieved for all the samples after sintering at 1350 ^{o}C for 4 hrs.
- Composition with x = 0.025 exhibits higher ionic conductivity than that of ceria doped singly with La and almost equal to the best reported values for $Ce_{0.8}Sm_{0.2}O_{1.9}$ and $Ce_{0.8}Gd_{0.2}O_{1.9}$ at 600 ^{o}C. This makes it a potential candidate as a solid electrolyte for IT-SOFCs being much cheaper.

5.2 Nanocomposites of La and Sr Co-Doped ceria (CL125S025)

5.2.1 Introduction

Recently, ceria/salt based nanocomposite solid electrolytes have been proved to be promising candidates for LT-SOFCs [Zhu et al. (2001); Zhu (2003); Zhu et al. (2004); Zhu et al. (2006)]. The interfaces formed between the two phases provide highways channels for transport of the ions. This leads to enhancement in the conductivity of the electrolytes. Transport efficiency depends on the two parameters; one is the interface density and second is the contact area between the two phases [Fan et al. (2013)]. In nanocomposite electrolytes, larger the interface area or grain boundaries area, higher will be the concentration of mobile defects in the space charge region [Arico et al. (2005)]. Single cell based on $Ce_{0.80}Sm_{0.20}O_{1.90}$/($Li_2CO_3$-$Na_2CO_3$) composite electrolyte showed a power density of 1700 mWcm^{-2} at a current density of 3000 mAcm^{-2} at 650 ^{o}C when CO_2/O_2 atmosphere was used at cathode [Xia et al. (2010)].

As mentioned in the above results, composition $Ce_{0.85}La_{0.125}Sr_{0.025}O_{1.9125}$ (CL125S025) shows the highest ionic conductivity (1.50×10^{-2} S/cm at 600 ^{o}C) of all the compositions. This value is higher than the highest values of conductivity reported for the compositions SDC and GDC at 600 ^{o}C. In the present section, nanocomposite electrolytes based on CL125S025/(Li-Na)$_2CO_3$ have been prepared and characterized by DTA, phases, microstructure, thermal expansion and electrical conductivity.

5.2.2 Results and Discussion

(a) Thermal analysis

Fig. 5.10 shows the DTA plots of all the composite samples. In the DTA plots, two endothermic peaks have been observed. One is around 100 ^{o}C which is due to evaporation of the adsorbed moisture in the sample. Second broad endothermic peak has been observed in the temperature range 486-490 ^{o}C. This is ascribed to melting of the binary carbonate mixture. As the carbonate content increases, second endothermic peak slightly shifts towards higher temperature. There is no exo or endothermic peak beyond 490 ^{o}C. Based on the DTA results, all the composite powders were calcined at 600 ^{o}C for 2 hrs.

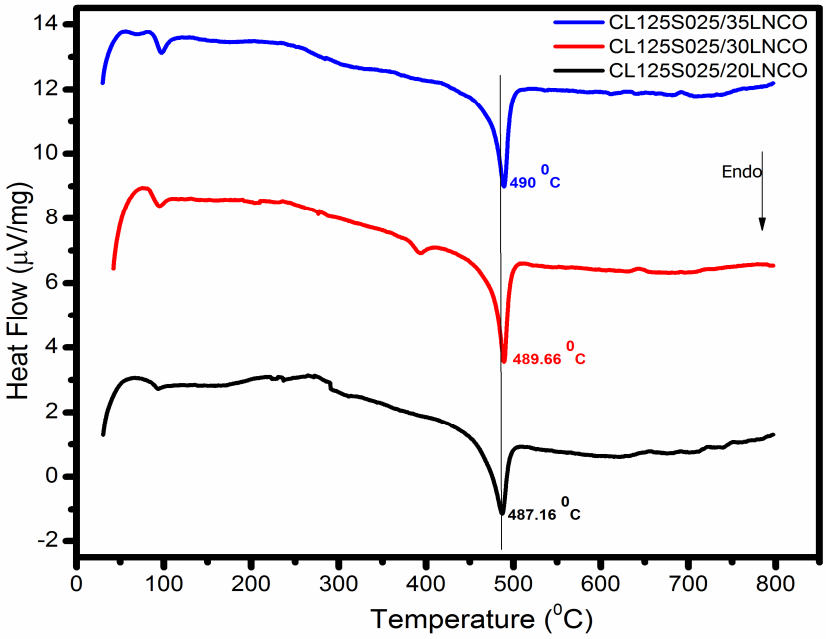

Fig. 5.10 DTA plots of all the composite samples of CL125S025/LNCO

(b) Crystal structure and phases

Powder X-ray diffraction patterns of all the milled (uncalcined), calcined and sintered samples are recorded to check the phase purity. Diffraction peaks have been indexed on the basis of JCPDS file no. 43-1002 for ceria. XRD patterns of all the sintered composite samples along with CL125S025 are shown in Fig. 5.11.

There is no peak of Li_2CO_3 and Na_2CO_3 i.e. carbonates are present in the amorphous state throughout the sample. Diffraction patterns of the milled powder (uncalcined) are the same as that of the calcined and sintered samples except that peaks are broad in the case of milled samples. Average particle size of the milled composite powders (uncalcined) has been found to be in the range 19-23 nm using Scherrer's formula. Nanosize particles will produce large interfacial region for conduction of the ions.

Density of the composites has been found to be in the range 82-85% of the theoretical value. This low value of density is due to very low sintering temperature 700 ^{o}C. Carbonates melt at the working temperature which fills in the interspaces between the ceria particles. This consequently enhances the density and work as a seal to avoid crossover of the gases [Di et al. (2010)].

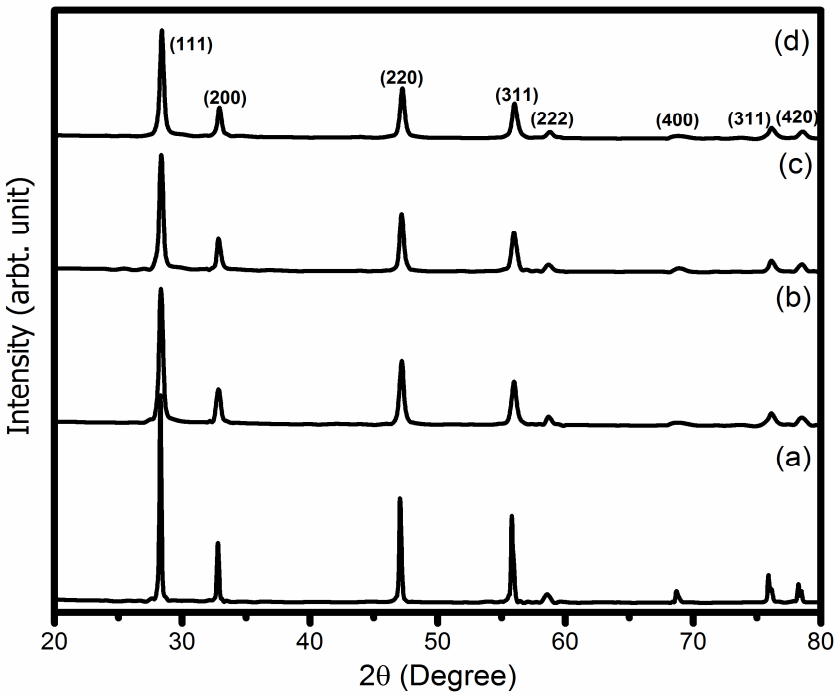

Fig. 5.11 XRD patterns of all the sintered powders of compositions (a) CL125S025 (b) CL125S025/20LNCO (c) CL125S025/30LNCO and (d) CL125S025/35LNCO

(c) Thermal expansion

Thermal expansion curve of the composites are shown in Fig. 5.12. It is noted that thermal expansion increases linearly up to 623 K. A change in the slope has been observed above this temperature. This is ascribed to the softening of the carbonate phase. The transition point (623 K) is less than that of melting temperature of the carbonates. It is consequence of the capillary forces due to surface tension which comes into play because of presence of smaller pores among the ceria particles throughout the matrix.

Table. 5.4 Coefficient of thermal expansion (CTE) of all the composites

S. No.	Compositions	CTE (K^{-1})
1.	CL125S025/20LNCO	14.30×10^{-6}
2.	CL125S025/30LNCO	14.40×10^{-6}
3.	CL125S025/35LNCO	16.70×10^{-6}

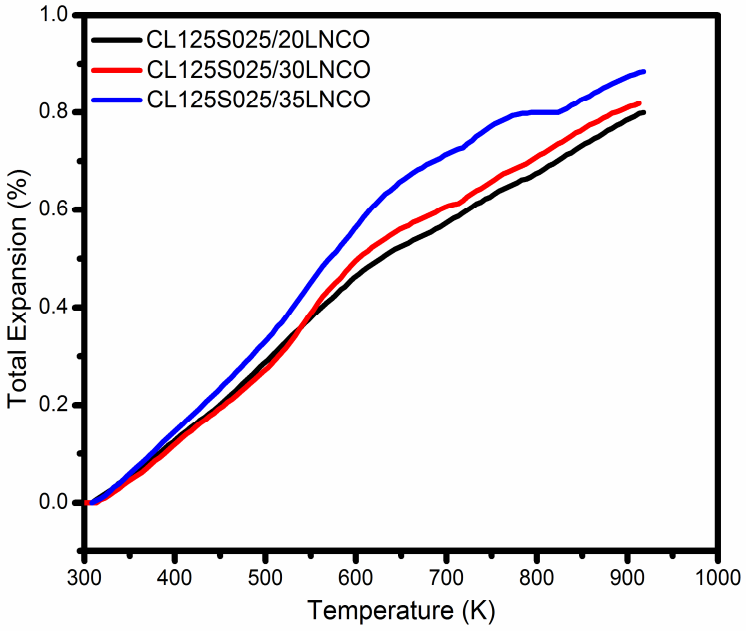

Fig. 5.12 Thermal expansion curves for CL125S025/LNCO nanocomposites

Values of CTE of all the samples are given in Table. 5.4. Compositions, CL125S025/20LNCO and CL125S025/30LNCO have nearly the same values of CTE and CL125S025/35LNCO has the highest CTE.

(d) Microstructure

Fig. 5.13 shows the SEM micrographs of all the sintered samples. It is observed from Fig. 5.13(a) that CL125S025 (sintered at 1350 °C) shows very dense structure with distinct grains and grain boundaries.

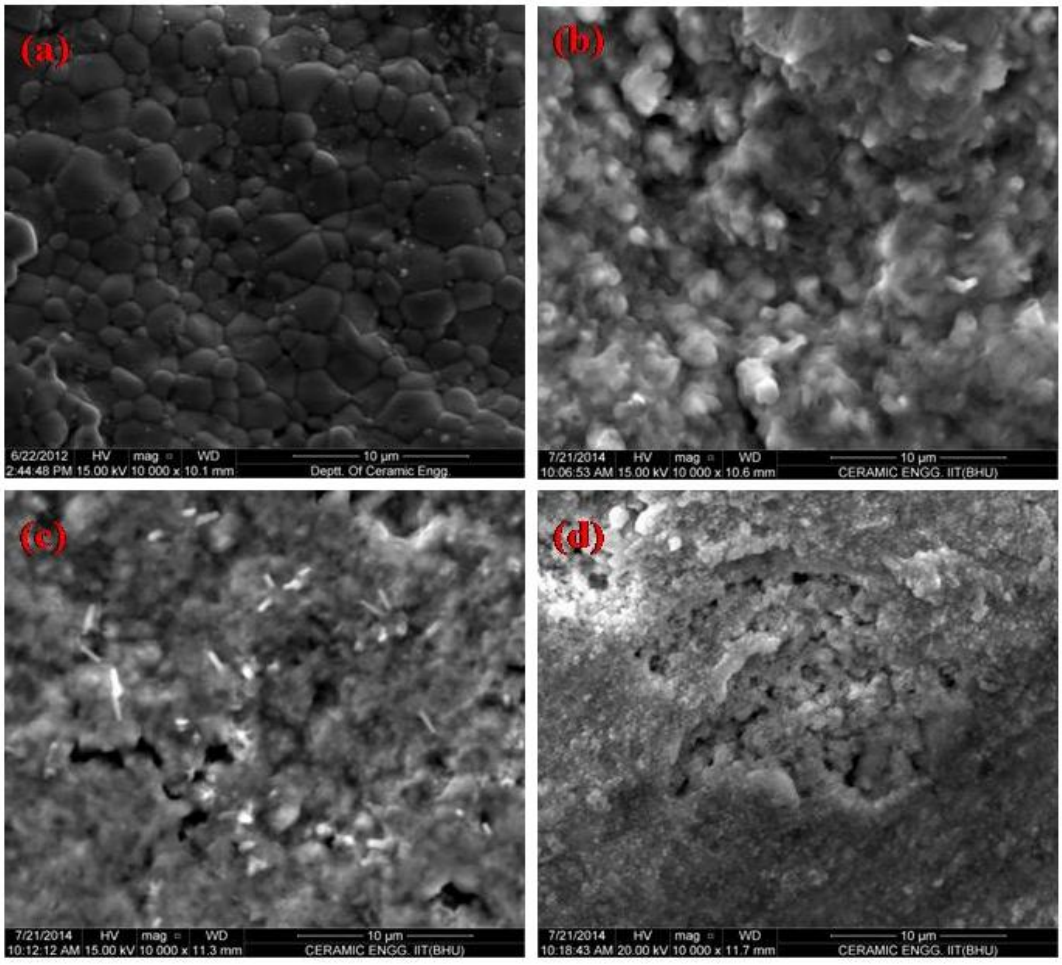

Fig. 5.13 SEM micrographs of all the sintered samples (a) CL125S025 (b) CL125S025 /20 LNCO (c) CL125S025/30 LNCO and (d) CL125S025/35 LNCO

It can also be seen from Figs. 5.13 (b)-(d) that CL125S025 particles are surrounded by molten carbonate amorphous phase. SEM micrographs of nanocomposites reveal that the size of CL125S025 particles is less than 100 nm. Due to presence of the large pores between the ceria grains, percolation of the carbonate phase is obvious. This microstructure may create large interfacial region for the conduction of ions. EDS spectrum of the composition, CL125S025/35LNCO, at two different points is shown in Fig. 5.14. All the elements are present in the expected concentration except Li. It is noted from the spectrum that the light grey region (spectrum 9) represents the crystalline ceria phase containing higher concentration of heavy cations. The higher contrast region (dark region, spectrum 10) represents the amorphous carbonate phase containing less concentration of heavy cations.

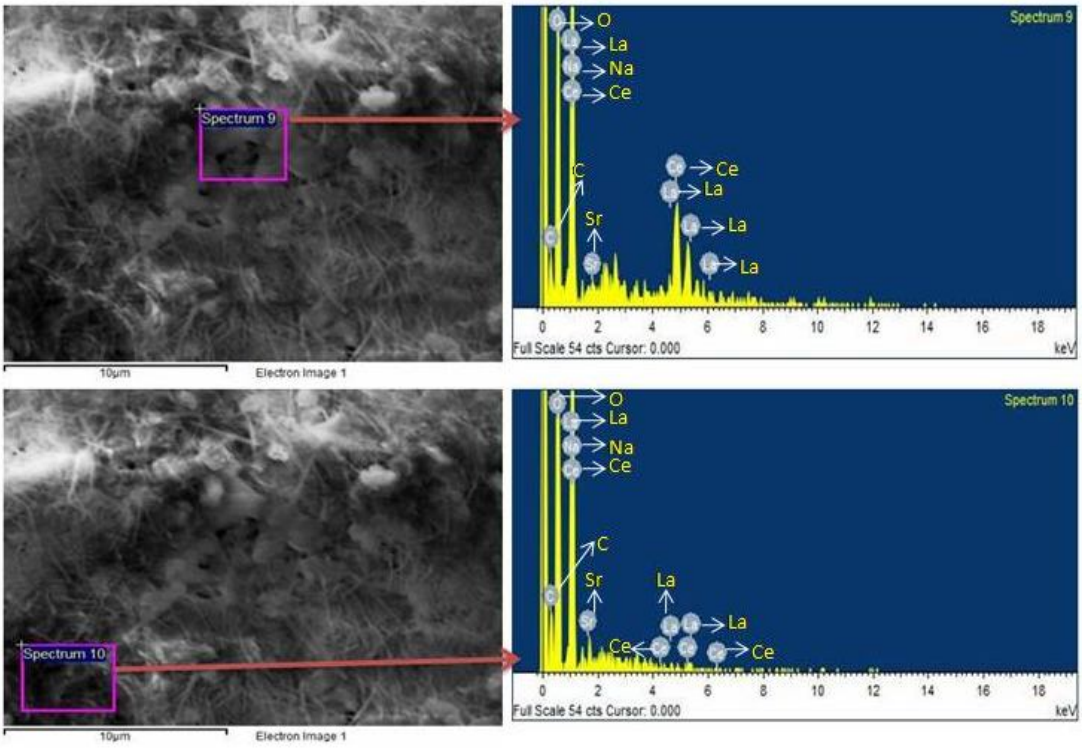

Fig. 5.14 EDS of the composition CL125S025/35LNCO at two different points

(e) Electrical conductivity

Electrical conductivity of all the samples has been determined using complex plane impedance analysis. Figs. 5.15 to 5.17 show the complex plane impedance plots of the composite samples at different temperatures. For composition, CL125S025/20LNCO, two depressed arcs along with a spike at lower frequency has been observed in the temperature range 200-250 ºC. A high frequency arc ascribed to the contribution of the grains and the arc observed in the intermediate frequency range corresponds to the contribution of the grain boundaries to the total resistance of the sample. A low frequency spike is due to electrode/electrolyte interface polarization. Arcs of the grains and the grain boundaries disappear above 250 and 375 ºC respectively due to increase in the relaxation frequency. An arc due to mass transfer process has been observed at 500 ºC in the lower frequency range. Arcs of the grains and the grain boundaries are associated with the capacitances in the pF (10^{-10}-10^{-12}) and nF (10^{-7}-10^{-9}) ranges respectively. These are determined from the relation $2\pi f_{max}RC = 1$, where f_{max} is the frequency at the highest point of the arc and R is the resistance and C is the capacitance of a particular contribution [Hodge et al. (1976)].

In case of the compositions, CL125S025/30LNCO and CL125S025/35LNCO, grains and grain boundaries arcs disappear above 250 and 300 ºC respectively. Only arcs due to electrode and mass transfer processes have been observed at higher temperatures. The sum of resistance of the grains and the grain boundaries is equal to the total resistance of the sample. Therefore, only arcs of the grains and the grain boundaries are fitted to determine the total resistance of the sample. The arc due to electrode is not fitted. The intercept on the real $Z^{'}$ axis at higher frequency side of the electrode arc has been considered as total resistance of the electrolyte at higher temperatures (when the arcs due to grains and grain boundaries disappear).

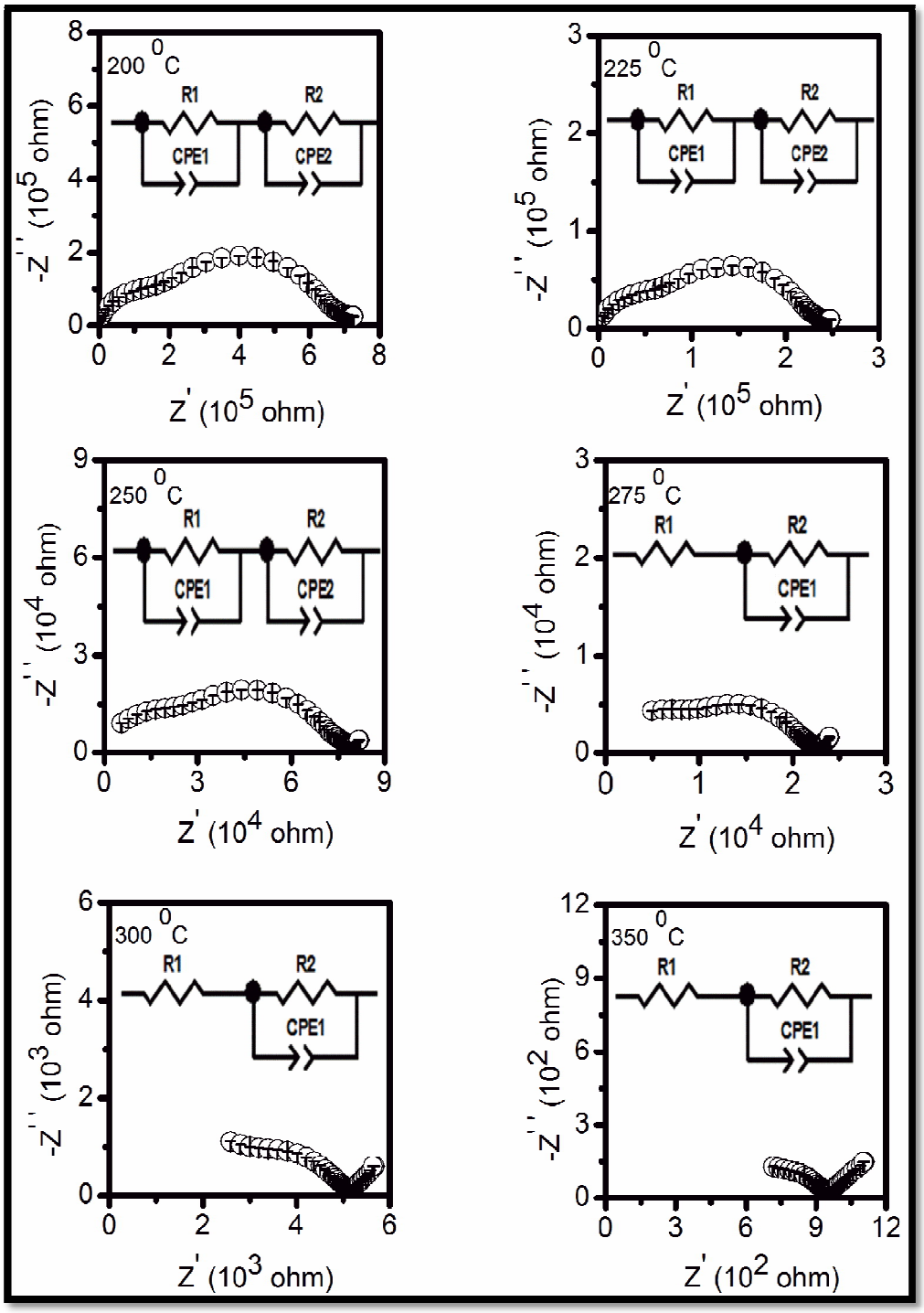

Fig. 5.15 Complex plane impedance plots of the composition CL125S025/20LNCO at different temperatures

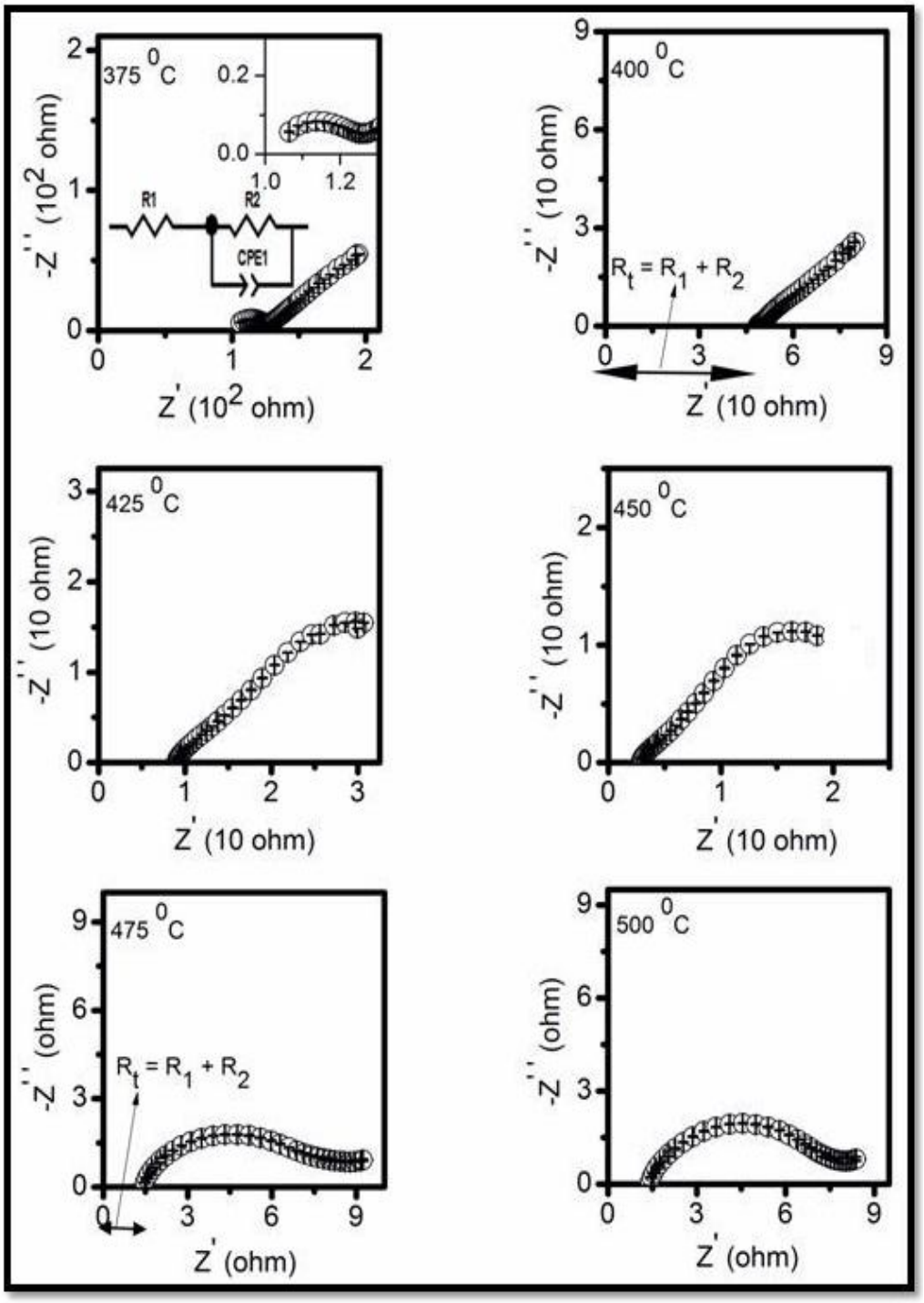

Fig. 5.15 Complex plane impedance plots of the composition CL125S025/20LNCO at different temperatures

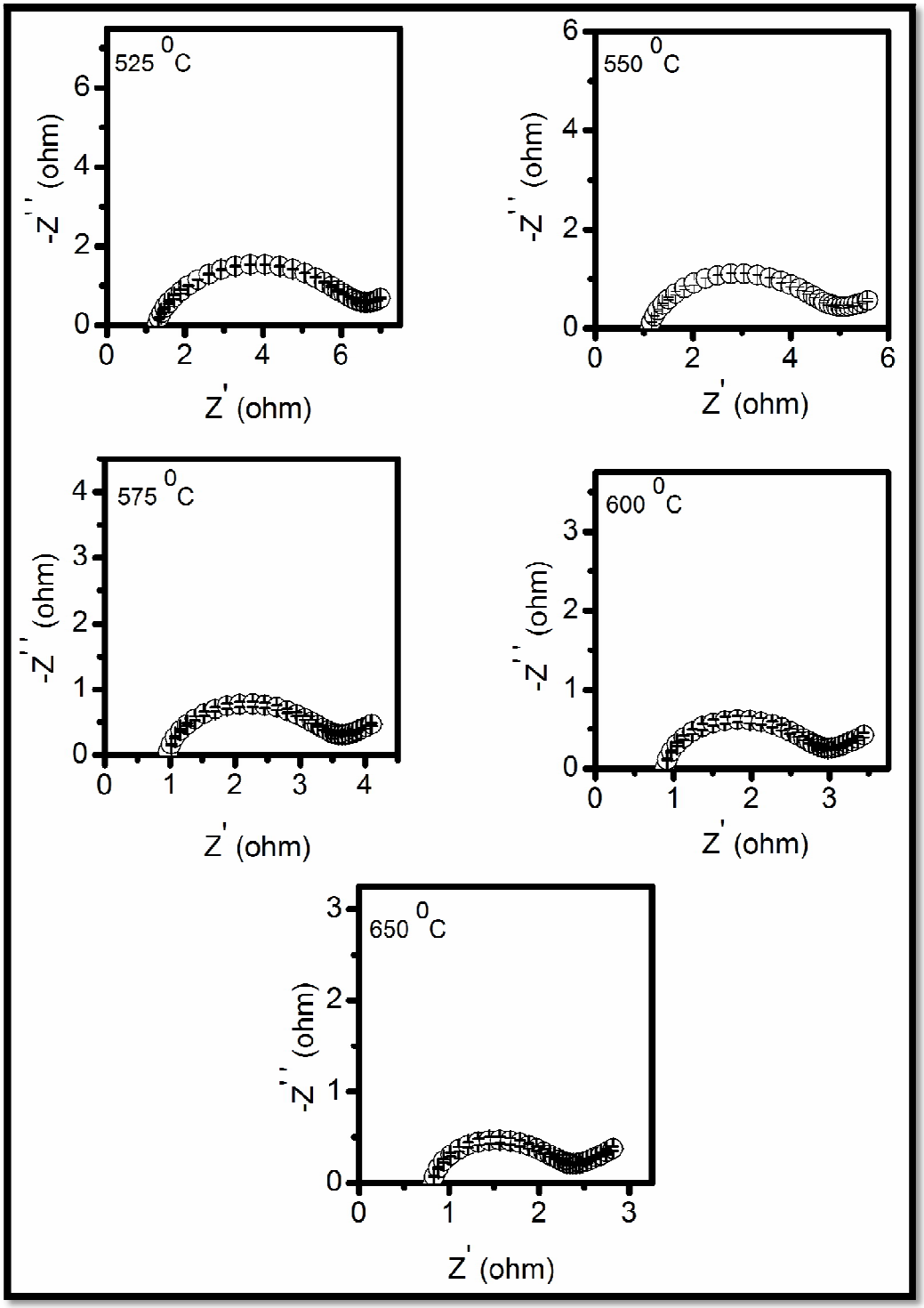

Fig. 5.15 Complex plane impedance plots of the composition CL125S025/20LNCO at different temperatures

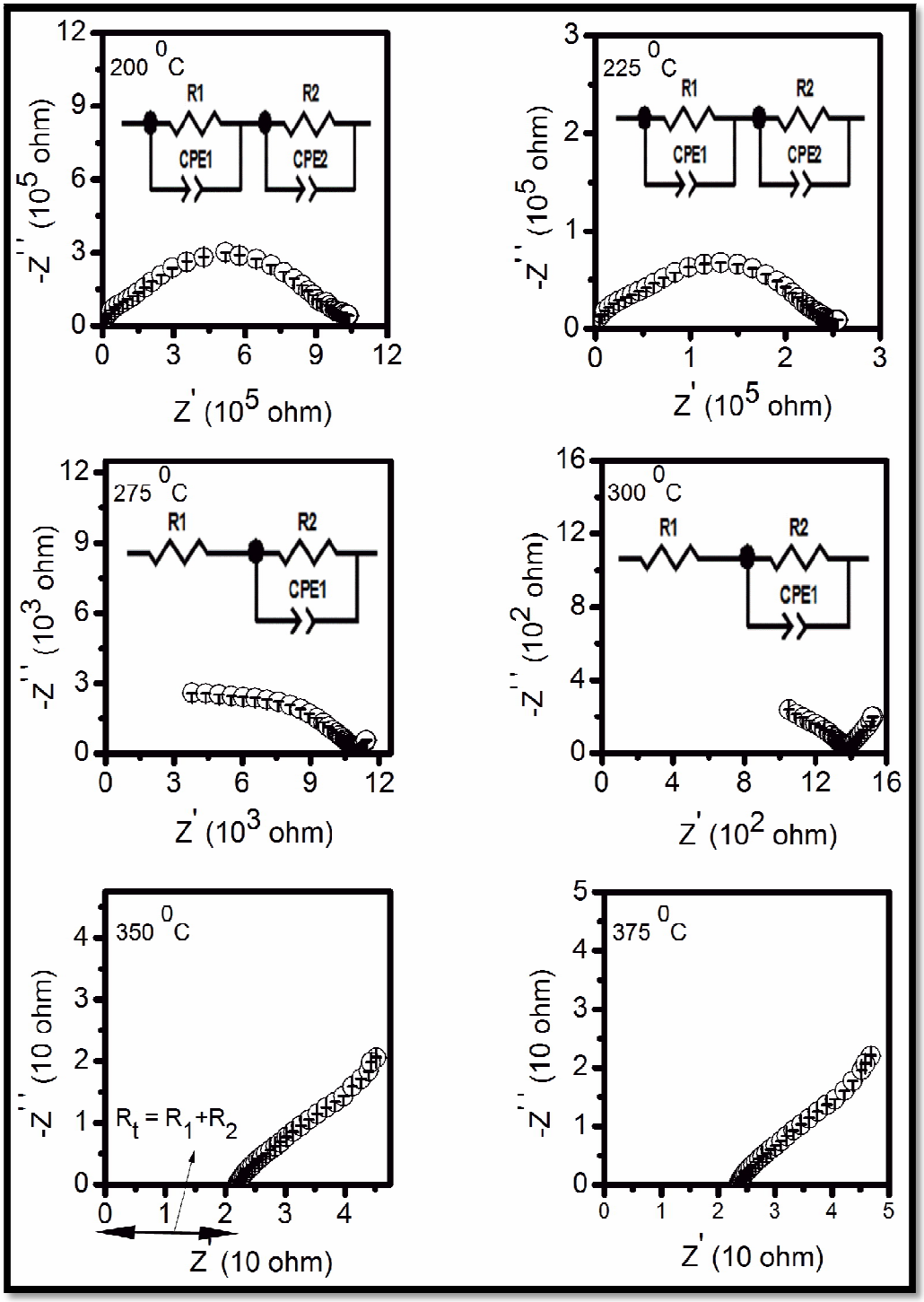

Fig. 5.16 Complex plane impedance plots of the composition CL125S025/30LNCO at different temperatures

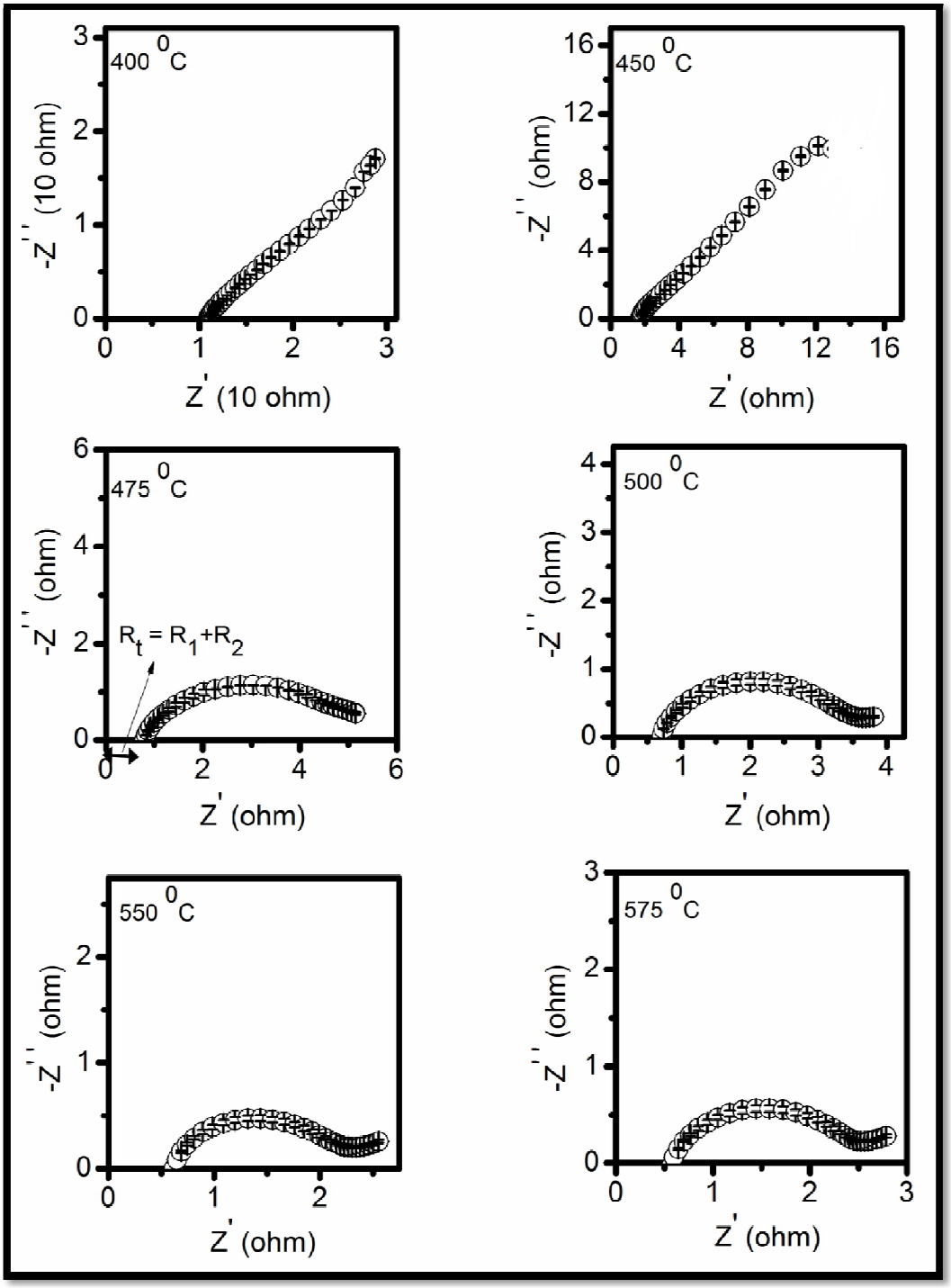

Fig. 5.16 Complex plane impedance plots of the composition CL125S025/30LNCO at different temperatures

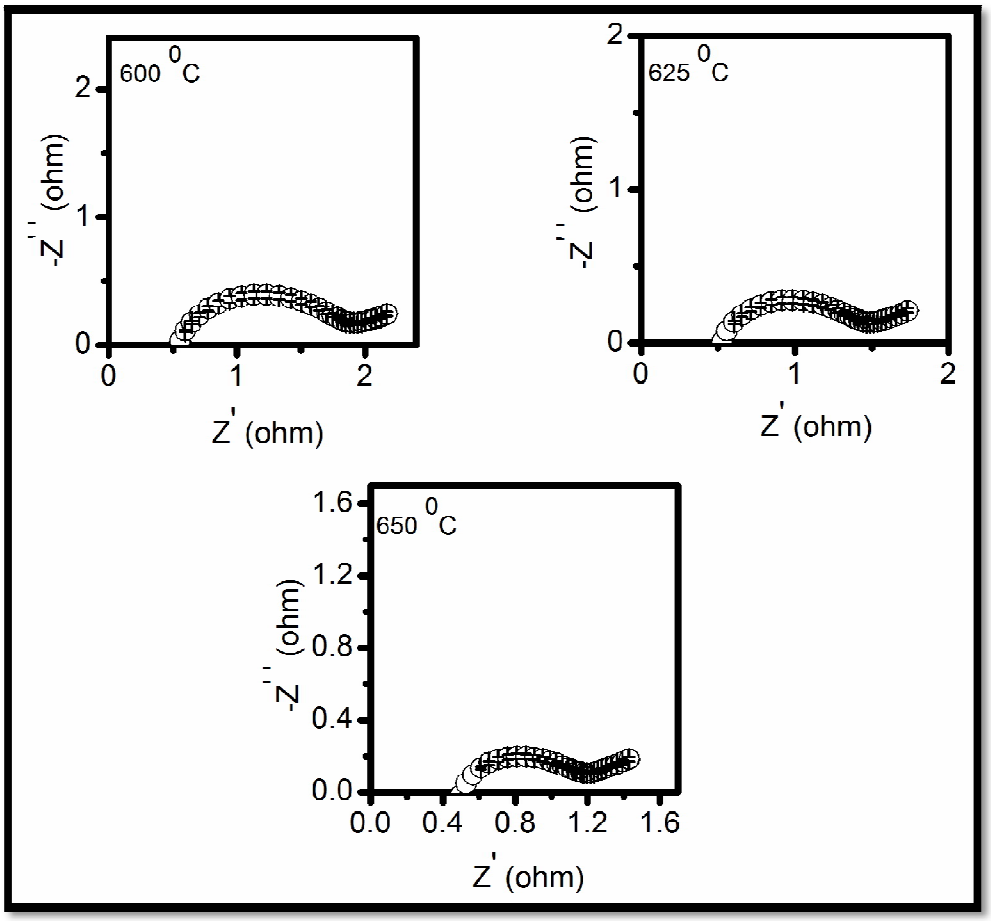

Fig. 5.16 Complex plane impedance plots of the composition CL125S025/30LNCO at different temperatures

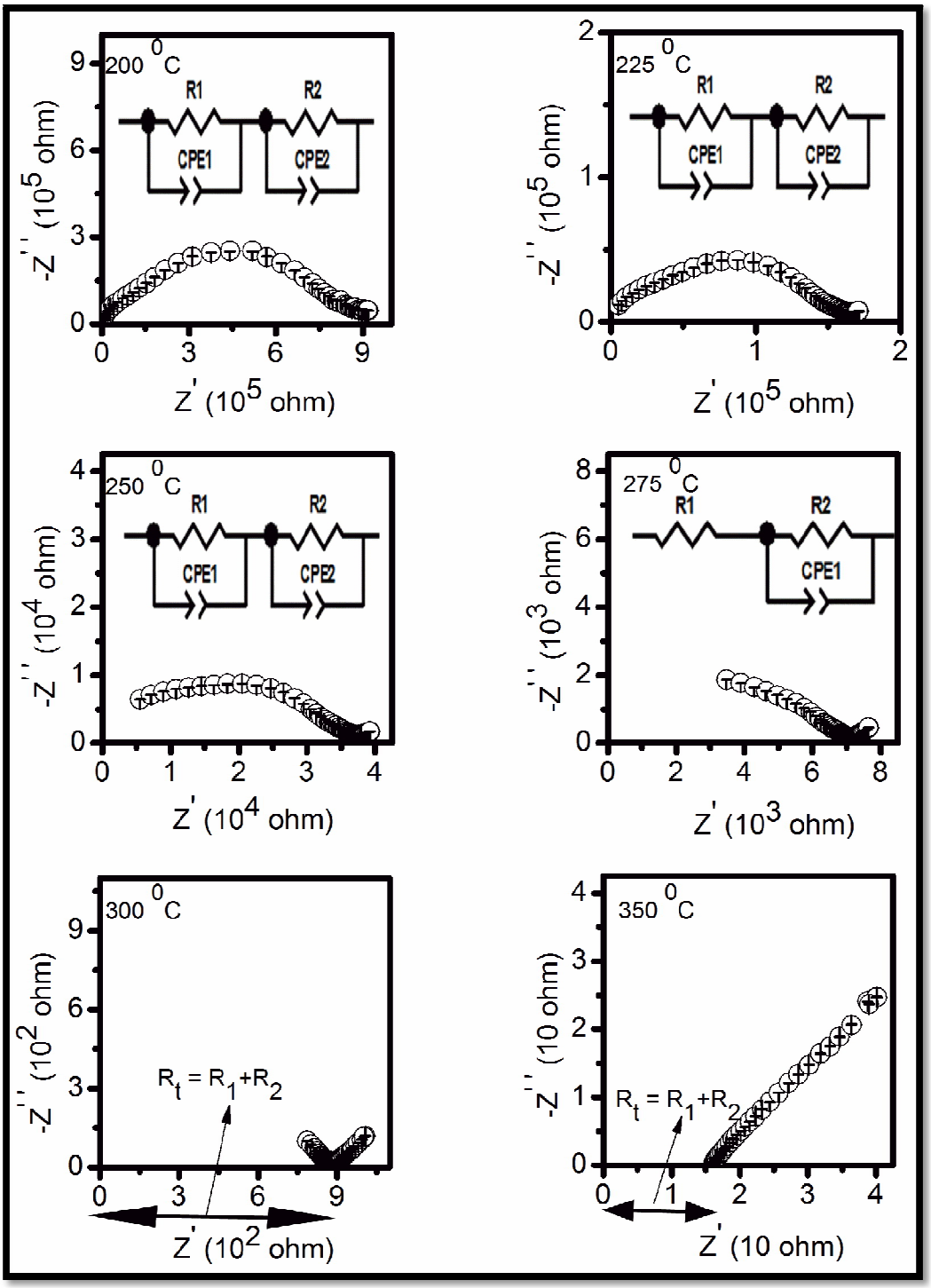

Fig. 5.17 Complex plane impedance plots of the composition CL125S025/35LNCO at different temperatures

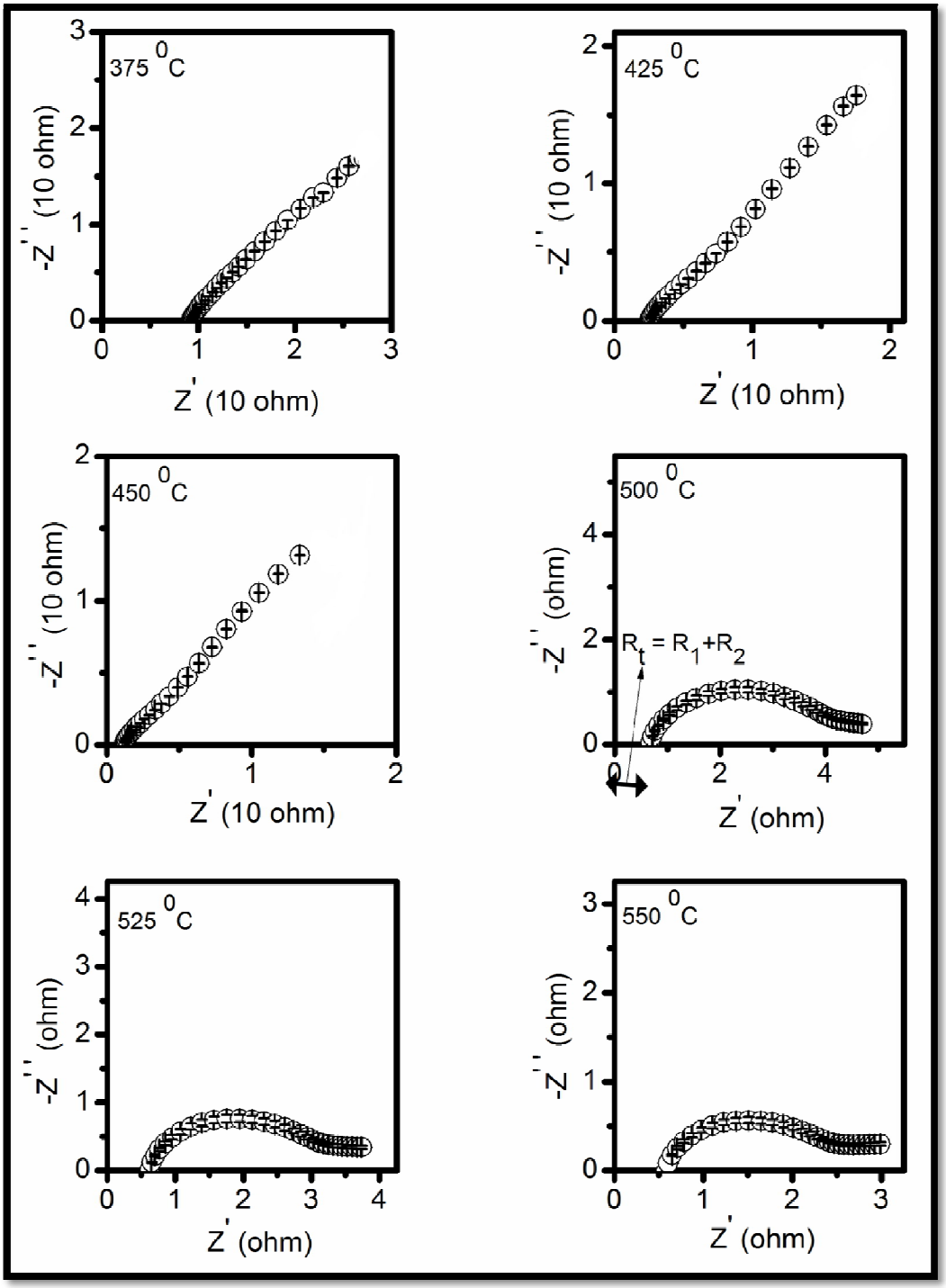

Fig. 5.17 Complex plane impedance plots of the composition CL125S025/35LNCO at different temperatures

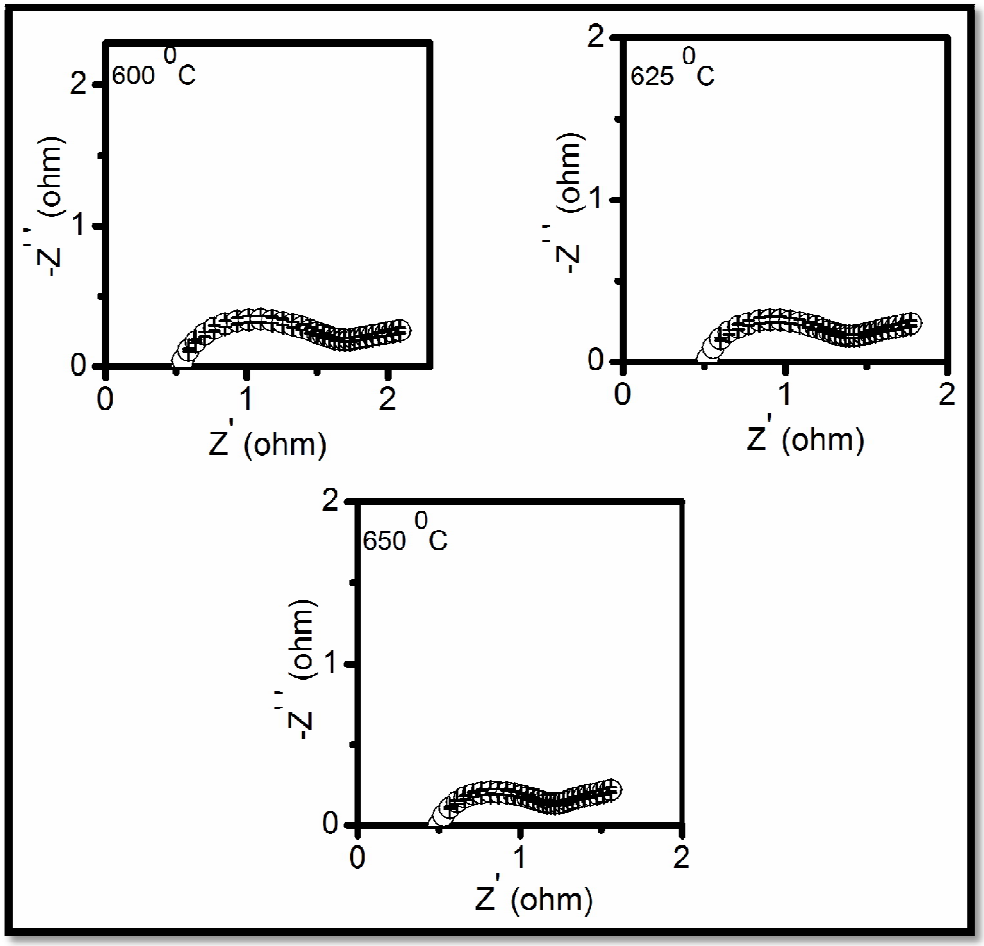

Fig. 5.17 Complex plane impedance plots of the composition CL125S025/35LNCO at different temperatures

Fig. 5.18 shows Arrhenius plots for the total ionic conductivity of the composites as well as CL125S025 and pure LNCO. Enhancement in the conductivity with the carbonate content (at higher temperatures) is evidenced by the plots in the insets. A jump in the conductivity plots has been observed for the composites around 350 °C. This corresponds to a superionic transition at the interfaces due to interfacial interaction between the two phases. It is the cause of existence of an electric field between the oppositely charged ions of the ceria phase and the carbonate phase [Zhu et al. (2008)].

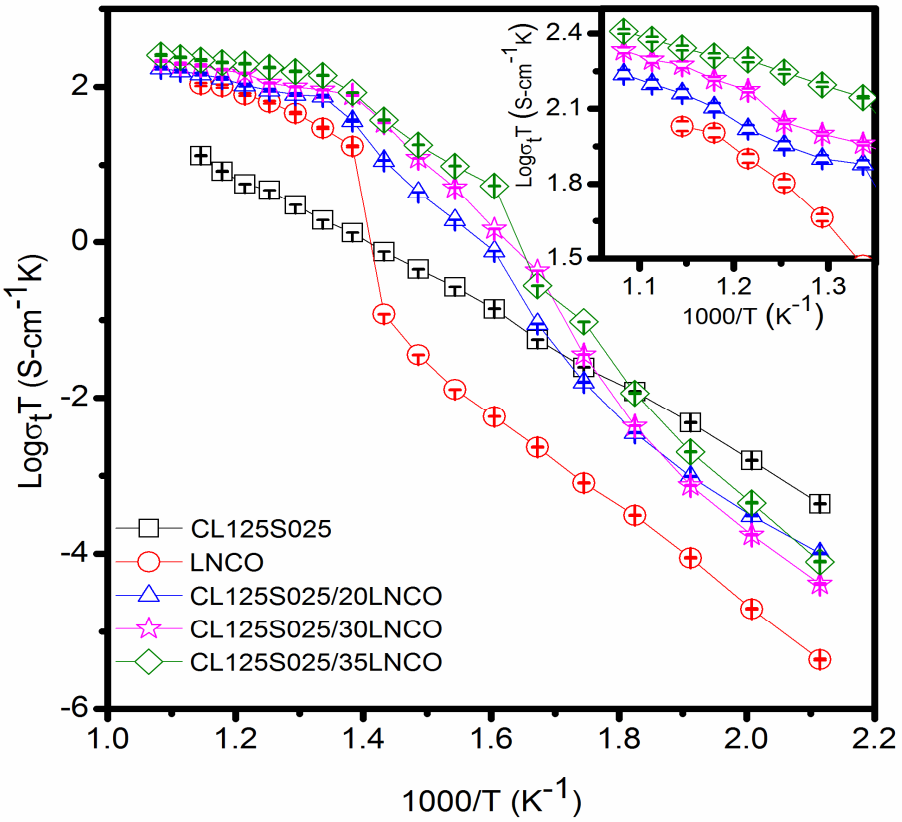

Fig. 5.18 Arrhenius plots of total conductivity for all the compositions in the system CL125S025/LNCO

The transition temperature is about 100 °C below the melting point of the carbonate (as seen in the DTA plots). This is because of percolation threshold causes a sudden increase in the conductivity below the melting temperature of the carbonates. Due to interfacial interaction between the two phases, a space charge zone is formed at the interfaces. In the space charge zone, concentration of cationic defects is higher than that in the bulk. Mobility of these defects increases due to melting from the sublattice to the bulk. Above the transition temperature, mobility of various ions such as Na^+, Li^+, H^+ and CO_3^{2-} leads to superionic conduction. Conductivity of the composites increases with increasing the carbonate content and it is higher than that of CL125S025 and LNCO above the transition temperature.

This is due to increase in the number of paths for the transport of the ions. In the nanocomposites, oxide ions conduct through the interfaces as well as in the bulk. Conductivity of all the compositions at 500 ^{o}C is given in Table. 5.5. Composite with 35 wt% of carbonate shows the conductivity, 0.203 S/cm at 500 ^{o}C with an activation energy of conduction 0.19 eV. This value is two orders of magnitude higher than that of 3.91×10^{-3} S/cm observed for the composition, CL125S025 at the same temperature. At 475 ºC, CL125S025/35LNCO has a conductivity 0.186 S/cm which is one order of magnitude more than 0.01 S/cm observed in $Ce_{0.8}Sm_{0.1}Nd_{0.1}O_{1.9}/(Li/Na)_2CO_3$ by Liu et al. at 481 ºC [Liu et al. (2010)]. Use of this composition, CL125S025/35LNCO, as a solid electrolyte for LT-SOFCs will reduce the cost as compared to using $Ce_{0.8}Sm_{0.1}Nd_{0.1}O_{1.9}/(Li/Na)_2CO_3$ because La^{3+} is cheaper than Sm^{3+}. Activation energy of conduction (E_a) and pre-exponential factor (σ_0) have been determined by fitting the conductivity data points to the Arrhenius equation:

$$\sigma = \sigma_0 \, exp\left(\frac{-E_a}{kT}\right) \tag{5.4}$$

Table. 5.5 Total conductivity at 500 ºC, activation energy and pre-exponential factor (σ_0) for all the compositions

S. No.	Compositions	σ_t at 500 $^{\circ}$C (S/cm)	E_a (200-450 $^{\circ}$C) eV	E_a (500-650 $^{\circ}$C) eV	σ_0
1.	CL125S025	3.91×10^{-3}	0.91 (200-600 $^{\circ}$C)		2.36×10^{06}
2.	LNCO	4.73×10^{-2}	1.26 (<500 $^{\circ}$C)	0.30 (>500 $^{\circ}$C)	3.05×10^{06}
3.	CL125S025/ 20LNCO	1.03×10^{-1}	1.50	0.31	1.82×10^{10}
4.	CL125S025 /30LNCO	1.20×10^{-1}	1.56	0.22	2.75×10^{10}
5.	CL125S025 /35LNCO	2.03×10^{-1}	1.63	0.19	3.47×10^{10}

It can be noted from Eq. 5.4 that the conductivity can be enhanced either by increasing σ_0 or decreasing E_a. Values of E_a at higher and lower temperatures and pre-exponential factor (σ_0) for all the compositions are given in Table.5.5. In the case of the composites, E_a is more at lower temperature and vice-versa. This is due to blocking of the mobile ions by dispersed solid carbonate amorphous phase at low temperature. Above the transition temperature, interfacial conduction of the ions causes low activation energy as compared to the bulk conduction [Zhu et al. (2008)]. It is noted from Table. 5.5 that composites have high value of σ_0 than that of CL125S025 and LNCO i.e. concentration of the mobile defects is higher in the composites.

Variation of conductivity in the nanocomposites with the carbonate content is given by Archie plot. Fig. 5.19 shows the Archie plot of the composite in the system CL125S025/LNCO. It shows that the ratio, $\sigma/\sigma_0^{'}$ (ratio of conductivity of composite to the conductivity of pure carbonate mixture) increases with increasing the carbonate content. Archie plot of CL125S025/LNCO composites lost linearity and bends towards lower normalized conductivity.

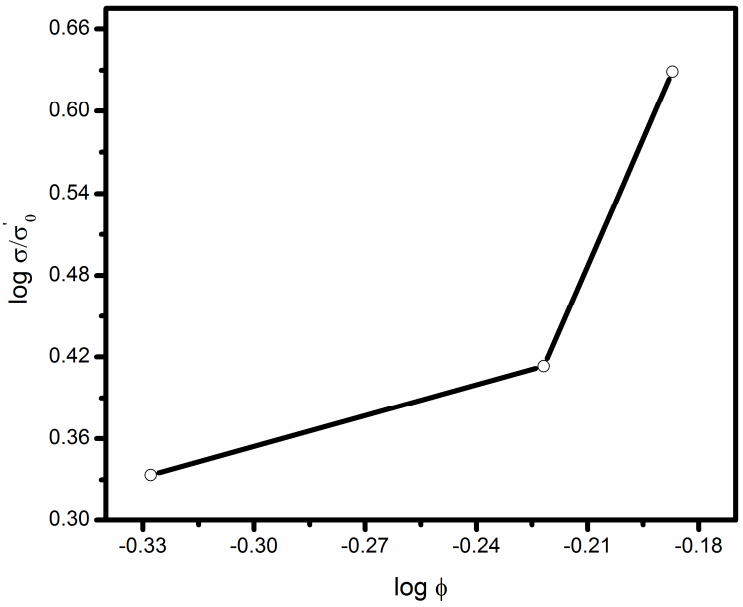

Fig. 5.19 Arhie plot of the system CL125S025/LNCO

5.2.3 Conclusion

- Nanocomposites in the system, $Ce_{0.85}La_{0.125}Sr_{0.025}O_{1.9125}$ with varying amount of binary mixture of carbonates $(Li\text{-}Na)_2CO_3$ have been prepared successfully by mixing nanocrystalline $Ce_{0.85}La_{0.125}Sr_{0.025}O_{1.9125}$ powder with the binary mixture of $(Li\text{-}Na)_2CO_3$.
- Ceria based single phase formation has been observed in all the composites.
- Micrographs show continuous distribution of both the phases with ceria grains surrounded by the carbonate amorphous phase.
- Impedance analysis shows that the charge transport in the composites is different from that in the ceria based electrolytes.
- A sharp increase in the conductivity has been observed around 350 ^{o}C. This is attributed to superionic transition at the interfaces.
- The composition, CL125S025/35LNCO shows the maximum conductivity, 2.03×10^{-1} S/cm at 500 ^{o}C.
- Activation energy of conduction of the composition CL125S025/35LNCO is found to be 0.19 eV which is ascribed to the interfacial conduction of the ions in the nanocomposites.
- These features may make this composite useful for application in LT-SOFCs (500 ºC).